

Oil & Natural Gas Technology

DOE Award No.: DE-FC26-04NT15526

Final Report

Transformation of Resources to Reserves: Next Generation Heavy-Oil Recovery Techniques

Submitted by:
Stanford University
Department of Energy Resources Engineering
Green Earth Sciences BLDG, room 065
367 Panama St
Stanford, CA 94305-2220

Prepared for:
United States Department of Energy
National Energy Technology Laboratory

March 28, 2008



Office of Fossil Energy



Disclaimer

This report was prepared as an account of work sponsored by an agency of the United States Government. Neither the United States Government nor any agency thereof, nor any of their employees, makes any warranty, express or implied, or assumes any legal liability, or responsibility for the accuracy, completeness, or usefulness of any information, apparatus, product, or process disclosed, or represents that its use would not infringe privately owned rights. Reference herein to any specific commercial product, process, or service by trade name, trademark, manufacturer, or otherwise does not necessarily constitute or imply endorsement, recommendation, or favoring by the United States Government nor any agency thereof. The views and opinions of the authors expressed herein do not necessarily state or reflect those of the United States Government nor any agency thereof.

Acknowledgements

Financial support for research in the area of heavy oil and thermal recovery mechanisms was provided by the U. S. Department of Energy under Award No. DE-FC26-04NT15526.

Contributions from the Stanford University Petroleum Research Institute (SUPRI-A) Industrial Affiliates: Aera Energy LLC, Berry Petroleum, BP Exploration, ChevronTexaco, ConocoPhillips, Riped PetroChina, Shell International Exploration & Production, Total, Tyco Thermal Controls are likewise acknowledged gratefully.

Assistance in chemical analyses of crude oils was provided by Dr. J. S. Buckley and Mr. T. Fan.

Contributors to this work include Dr. L.M. Castanier, Mr. Q. Chen, Prof. A. R. Kavscek, Ms. L. Liang, Ms. W. Lin, Dr. G.-Q. Tang, and Mr. C. Temizel,

Executive Summary

This final report and technical progress report describes work performed from October 1, 2004 through September 30, 2007 for the project "Transformation of Resources to Reserves: Next Generation Heavy Oil Recovery Techniques," DE-FC26-04NT15526. Critical year 3 activities of this project were not undertaken because of reduced funding to the DOE Oil Program despite timely submission of a continuation package and progress on year 1 and 2 subtasks. A small amount of carried-over funds were used during June-August 2007 to complete some work in the area of foamed-gas mobility control. Completion of Year 3 activities and tasks would have led to a more thorough completion of the project and attainment of project goals.

This progress report serves as a summary of activities and accomplishments for years 1 and 2. Experiments, theory development, and numerical modeling were employed to elucidate heavy-oil production mechanisms that provide the technical foundations for producing efficiently the abundant, discovered heavy-oil resources of the U.S. that are not accessible with current technology and recovery techniques. Work fell into two task areas: cold production of heavy oils and thermal recovery. Despite the emerging critical importance of the waterflooding of viscous oil in cold environments, work in this area was never sanctioned under this project.

It is envisioned that heavy oil production is impacted by development of an understanding of the reservoir and reservoir fluid conditions leading to so-called foamy oil behavior, i.e, heavy-oil solution gas drive. This understanding should allow primary, cold production of heavy and viscous oils to be optimized. Accordingly, we evaluated the oil-phase chemistry of crude oil samples from Venezuela that give effective production by the heavy-oil solution gas drive mechanism. Laboratory-scale experiments show that recovery correlates with asphaltene contents as well as the so-called acid number (AN) and base number (BN) of the crude oil. A significant number of laboratory-scale tests were made to evaluate the solution gas drive potential of West Sak (AK) viscous oil. The West Sak sample has a low acid number, low asphaltene content, and does not appear foamy under laboratory conditions. Tests show primary recovery of about 22% of the original oil in place under a variety of conditions. The acid number of other Alaskan North Slope samples tests is greater, indicating a greater potential for recovery by heavy-oil solution gas drive.

Effective cold production leads to reservoir pressure depletion that eases the implementation of thermal recovery processes. When viewed from a reservoir perspective, thermal recovery is the enhanced recovery method of choice for viscous and heavy oils because of the significant viscosity reduction that accompanies the heating of oil. One significant issue accompanying thermal recovery in cold environments is wellbore heat losses. Initial work on thermal recovery found that a technology base for delivering steam, other hot fluids, and electrical heat through cold subsurface environments, such as permafrost, was in place. No commercially available technologies are available, however. Nevertheless, the enabling technology of superinsulated wells appears to be realized.

Thermal subtasks focused on a suite of enhanced recovery options tailored to various reservoir conditions. Generally, electrothermal, conventional steam-based, and thermal gravity drainage

enhanced oil recovery techniques appear to be applicable to “prime” Ugnu reservoir conditions to the extent that reservoir architecture and fluid conditions are modeled faithfully here.

The extent of reservoir layering, vertical communication, and subsurface steam distribution are important factors affecting recovery. Distribution of steam throughout reservoir volume is a significant issue facing thermal recovery. Various activities addressed aspects of steam emplacement. Notably, hydraulic fracturing of horizontal steam injection wells and implementation of steam trap control that limits steam entry into horizontal production wells overcomes many of the problems associated with implementation of thermal gravity drainage processes in heterogeneous sands. In a steam-assisted gravity drainage (SAGD) well pattern, hydraulically fractured injectors were able to achieve significantly improved reservoir heating and improvements to oil-steam ratio. On the opposite side of the steam injection spectrum, steam often channels through high-permeability zones. Foamed steam stabilized by aqueous surfactants is promising to alter steam flow, but has yet to be tested and simulated under SAGD conditions. The mechanistic population balance method for describing foam flow was extended to a local equilibrium framework that reduces computational costs and is promising for simulation of the effects of foamed steam in 3D. Other thermal recovery techniques of cyclic steam injection and electrical resistance heaters that are deployable in wellbores and in multilateral configurations are explored. This suite of techniques provides a range of recovery options that can be tailored to specific viscous and heavy oil conditions.

Table of Contents

<u>DISCLAIMER</u>	<u>I</u>
<u>ACKNOWLEDGEMENTS</u>	<u>II</u>
<u>EXECUTIVE SUMMARY</u>	<u>III</u>
<u>INTRODUCTION</u>	<u>1</u>
<u>APPROACH</u>	<u>2</u>
<u>RESULTS AND DISCUSSION</u>	<u>6</u>
1.1 COLD PRODUCTION– EXPERIMENTAL INVESTIGATION	6
1.2 COLD PRODUCTION– SIMULATION OF COLD PRODUCTION	10
2.1 THERMAL RECOVERY– REVIEW OF ADVANCED WELL COMPLETIONS	10
2.2 THERMAL RECOVERY– THERMAL GRAVITY DRAINAGE	10
2.3 THERMAL RECOVERY– COMPARISON OF CYCLIC STEAM INJECTION AND DOWNHOLE HEATING	24
2.4 THERMAL RECOVERY–FOAMED-GAS MOBILITY CONTROL	38
<u>MANAGEMENT ASPECTS AND DISCUSSION</u>	<u>51</u>
COST AND SCHEDULE STATUS	51
SUMMARY OF ACCOMPLISHMENTS	51
ACTUAL OR ANTICIPATED PROBLEMS	51
TECHNOLOGY TRANSFER ACTIVITIES	52
<u>CONCLUSION</u>	<u>53</u>
<u>REFERENCES</u>	<u>54</u>

Introduction

The United States relies more extensively on imported oil year by year. Over the past 25 years, U.S. petroleum consumption has grown at an average rate of 0.5% per year. The fraction of oil imported has grown from 28% of U. S. consumption in 1983 to about 60% today (EIA 2006). Yet, the current situation has not emerged because the U.S. lacks substantial oil and gas resources. Rather, we have not been successful at conducting the research and development to develop cost-effective production techniques that allow us to convert known resources into reserves. A case in point is heavy oil. Estimates place the total heavy resource (less than 20 °API) in the United States in the neighborhood of 200 billion bbl (Janisch 1979, Mahmood et al. 1995). At 2006 consumption rates, this resource represents a little more than 45 years of total oil supply for the U.S. It is also noteworthy that heavy-oil resources in the Western Hemisphere are well in excess of 5.5 trillion bbl whereas the oil resource of the Middle East is estimated as 1.4 trillion bbl.

Heavy oils are much more viscous than conventional oils. Consequently, they are difficult to produce. Reservoirs containing heavy oil differ in oil-phase viscosity and are located in a variety of settings: onshore, offshore, and in the Arctic. Thus, a suite of heavy-oil recovery methods is needed to address oil production across a broad range of conditions. The goal of this project was to provide midterm research that underpins the development of recovery technologies needed to produce efficiently the abundant, discovered heavy-oil resources of the U.S. This goal includes increasing heavy-oil recovery efficiency in an environmentally sound manner so that resources are utilized with minimum environmental impact and the amount of oil remaining at abandonment is minimized. The chief problem, of course, with heavy oil is economic exploitation of the resource. Thermal recovery, and steam injection in particular, is tremendously successful. To date, more than 4 billion bbl of oil have been recovered as a result of steam injection (Moritis 2002). Nevertheless, conventional steam injection candidates are limited to onshore, relatively shallow, thick, permeable, and homogeneous sands where benign surface conditions exist.

Work within this project was organized into broad task areas of (i) cold production and (ii) thermal recovery including mobility control of steam. The tasks embrace heavy-oil production from primary through to enhanced oil recovery. Tasks and subtasks included:

- Task 1 Cold Production
 - 1.1 Experimental Investigation
 - 1.2 Simulation of Cold Production
- Task 2 Thermal Recovery
 - 2.1 Review of advanced well completions
 - 2.2 Cyclic steam injection
 - 2.3 Comparison of cyclic steam injection, thermal gravity drainage, and downhole heating
 - 2.4 Foamed-gas mobility control

By way of background, cold production uses the solution gas drive mechanism to recover oil in primary mode. It is quite efficient in some heavy-oil settings because gas released from solution

remains dispersed within the pore space of the rock. A sizeable fraction of the gas liberated remains in the reservoir enhancing production during pressure depletion. A two-pronged approach was used for this task. Experiments were used to delineate a conceptual model of gas-phase growth and oil production mechanisms. The second part of the task was intended to formulate a mechanistic, full-featured simulator of cold production. This simulation subtask was to be completed in year 3. The knowledge gained from the experiments and the simulation model would have allowed optimization of heavy primary operations.

Secondary recovery via water injection is viable for some viscous and heavy oils (Vittoratos et al, 2006). Additionally, it is frequently perceived as the only recovery option for Arctic and offshore operations. High mobility ratio waterflooding, however, is beyond the scope of this work.

With respect to the thermal recovery task, heat is the principal means to reduce heavy-oil viscosity in situ and enhance well productivity. This task lays the technical foundations for transferring the commercially effective process of steam injection to Arctic and offshore conditions. A complete case was intended for thermal oil recovery from well completions to thermal gravity drainage mechanisms to mobility control of steam. Key components of this effort include numerical and analytical modeling of cyclic steam injection to determine recovery and the economic limit. A comparison of cyclic steam injection, thermal gravity drainage, and other methods of downhole heating to understand thermal efficiency and natural gas requirements for heat generation. Extensive research on aqueous foams for mobility control of steam was also planned as was the role of hydraulic fractures in improving injected steam distribution. We furthered our understanding of gas mobility during foam flow using experiments and theory development to improve our ability to engineer foamed-gas injection projects.

Approach

This research project addresses a spectrum of recovery techniques applicable to heavy oil. In this report, the approach has included (i) pressure depletion experiments to quantify the mechanisms of primary, viscous oil recovery, (ii) quantification of crude-oil chemistry via acid number measurements, (iii) experiments in two-dimensional etched silicon micromodels to visualize the mechanisms of foam generation by capillary snap off, (iv) numerical reservoir simulation to understand thermal oil production in heavy-oil reservoirs with poor vertical communication, and (iv) literature review.

The approach taken for Task 1.1 Experimental Investigation of Cold Production is that of chemical analysis of heavy oil and experiments to measure primary depletion behavior. Most chemical analyses of heavy oils focus on asphaltenes and the paucity of short-chain hydrocarbon components in the crude-oil mixture. Our analysis probed the functional groups presented by various hydrocarbon components. We also intended to ascertain whether such acid and base functional groups associated with the asphaltene fraction. The focus on acid functional groups arises because reaction of the acid groups with alkali is known to produce interface stabilizing surfactants. Secondly, we conduct primary depletion experiments in a specially designed coreholder, illustrated in Fig. 1 The experimental setup is similar to that reported previously (Akin and Kovscek, 2002) and so is not discussed here in further detail.

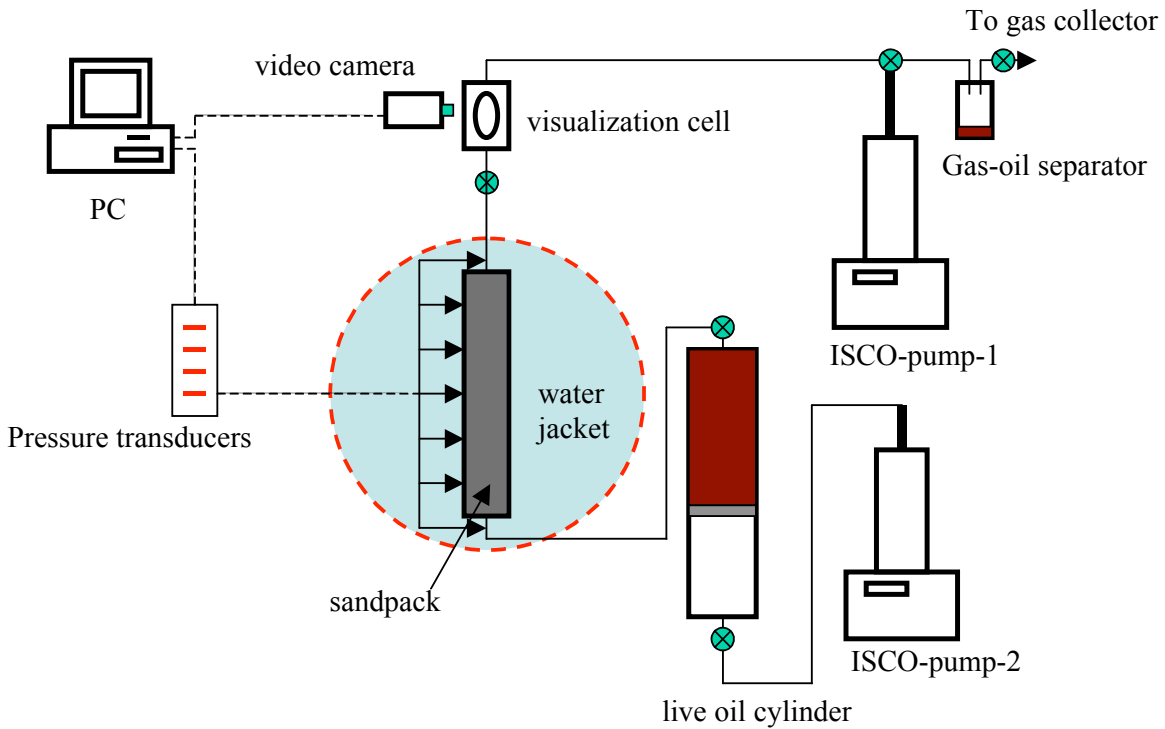


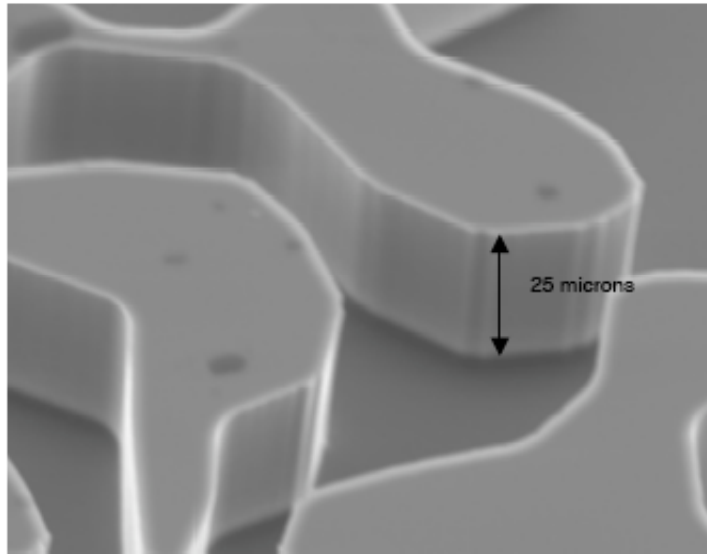
Figure 1. Experimental apparatus. Coreholder is heated/cooled using a circulating, temperature bath.

The approach planned for Task 1.2 was theory development through the synthesis of a conceptual and numerical model relevant to U.S. heavy oils. Because the effort for this project was reduced, this subtask was not pursued fully.

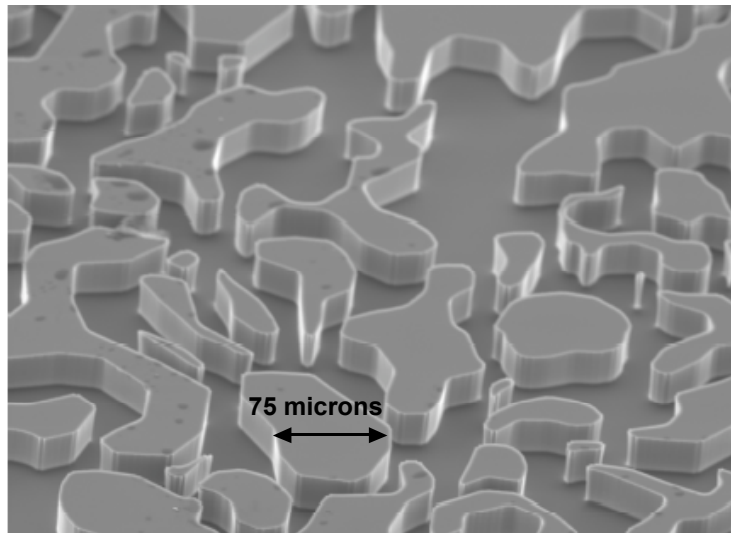
On the thermal recovery side of the project, The approach taken for Task 2.1 Advanced Well Completions is that of literature review. The main sources consulted were the technical paper database of the Society of Petroleum Engineers, a database of patent applications and patents granted, and other petroleum industry literature. Task 2.2 applies analytical modeling to make explicit the parameters leading to successful cyclic steam operations. The approach for Task 2.3 is numerical reservoir simulation to evaluate and screen various thermal recovery methods appropriate for viscous oil. The various options are explored using an appropriate thermal, compositional reservoir simulator (i.e., CMG STARS).

Ultimately, a variety of approaches were employed in Task 2.4 Foamed Gas Mobility Control as we built a mechanistic understanding and simulation framework to describe the physics of foam flow through porous media. Initial effort was placed on experiments in a microvisual apparatus to obtain new data relevant to foam generation by capillary snap off. Such data is needed to formulate accurate simulation models. Micromodels allow direct pore-scale observation of multiphase flow through porous media. They contain an etched flow pattern that is viewed with a microscope as shown in Fig. 2. Micromodels provide the best means to visualize fluid movement at the pore scale while honoring both geometric and topologic properties of real rocks. Etched-silicon-wafer micromodels of the type described by Sagar and Castanier (1998), initially developed by Hornbrook et al. (1991), were used for new studies. These micromodels contain a repeated pattern obtained from a scanning electron microscope image of a rock thin section, as shown in Fig. 2 for Berea sandstone. These micromodels offer 1:1 size scaling of typical sandstone pores. Note the grains appear as islands and the etched pores and throats as channels. The depth of flow channels is 25 μm and grains range in size from 30 to 200 μm , Fig. 2b. The porosity is roughly 0.2 and the permeability is approximately 500 mD. The total network dimension is 5-cm square. This represents a two-dimensional porous medium of 600 by 600 pores. The total number of pores appears to be sufficient to meet the requirements for representative elementary volume (REV) scaling (Dullien, 1992)

A holder to mount the micromodels for unobstructed viewing under the microscope was specially designed, Fig. 2. This aluminum (6061 T6) micromodel holder has conduits connected to the injection and production systems. There are four ports (one for each hole of the micromodel) that are sealed with viton O-rings, Fig. 3. Pore-level events are observed directly via microscope.



(a)



(b)

Figure 2. Scanning electron microscope (SEM) images of silicon micromodel: (a) close-up view to reveal depth of etching, sharp pore corners, and rough edges of pore walls and (b) etched network pattern.

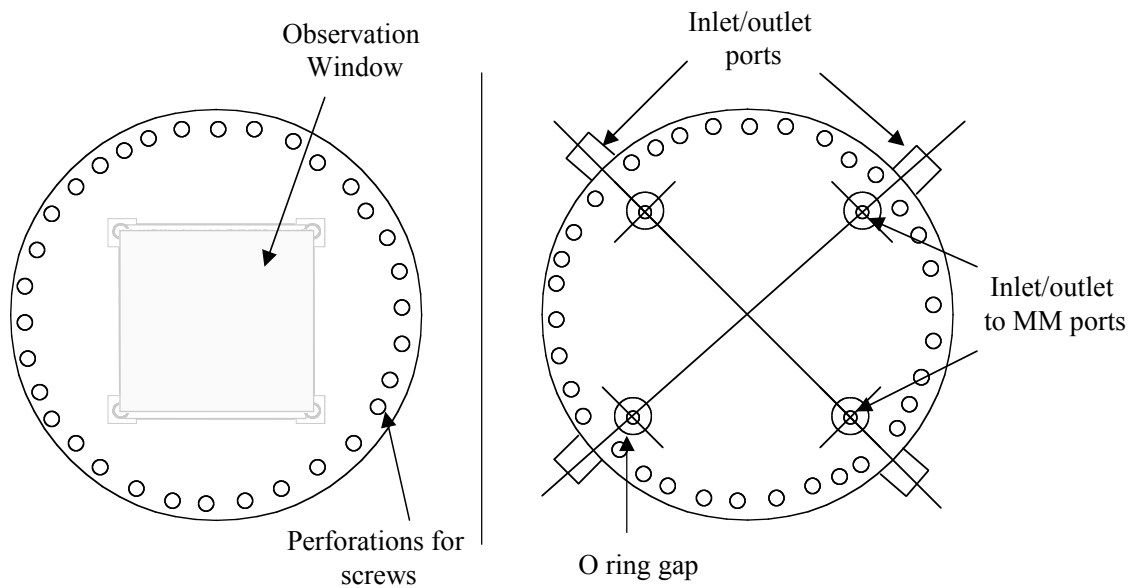


Figure 3. Schematic of the micromodel holder. Top (left) and bottom (right) pieces.

Results and Discussion

The presentation of results obtained during this project and discussion is broken down by task and subtask.

1.1 Cold Production– Experimental Investigation

Our main focus was to develop a suite of primary depletion data for viscous West Sak (AK) crude oil. In addition to developing a quantitative database of the production potential of viscous 20.5 °API West Sak crude, our aim was to develop an understanding of why gas bubbles remain dispersed in some viscous crude oils thereby contributing to favorable recovery.

Oil Chemical Analyses

We categorized heavy-oil functional groups by measuring the so-called acid and base numbers of viscous crude-oil samples. The acid number is the mass of base needed to neutralize a crude oil and is reported as the amount of KOH (ASTM, 2004). Figure 4(a) illustrates schematically a carboxylic acid functional group that is measured using the acid number. On the other hand, the base number is the amount of acid needed to neutralize a crude oil. A typical functional group that is probed by a measurement of base number is illustrated in Fig. 4(b). The presence of such groups correlates with foaming in distillation columns (Callaghan, et al., 1985) as well as interfacial activity in mineral processing (Zhou et al, 1999). Oil viscosity also clearly plays a role in retarding the coalescence of small gas bubbles into a continuous gas phase thereby aiding oil recovery (George et al., 2005) but crude-oil components, such as asphaltenes, incorporating carboxylic acid functional groups slows coalescence more significantly.

A number of depletion experiments were conducted with a solution gas oil ratio (GOR) of 20 whereas additional experiments were conducted at GOR equal to 40. Our results are presented in a recent paper (Tang et al, 2006). In both cases, depletion rates of 0.035 PV/hr and 0.0035 PV/hr, respectively, were employed. Typical data collected is displayed in Fig. 5. It plots average pressure in the sandpack as a function of the system expansion. Note the strong similarity in the results of each test despite the factor of 10 difference in depletion rate.

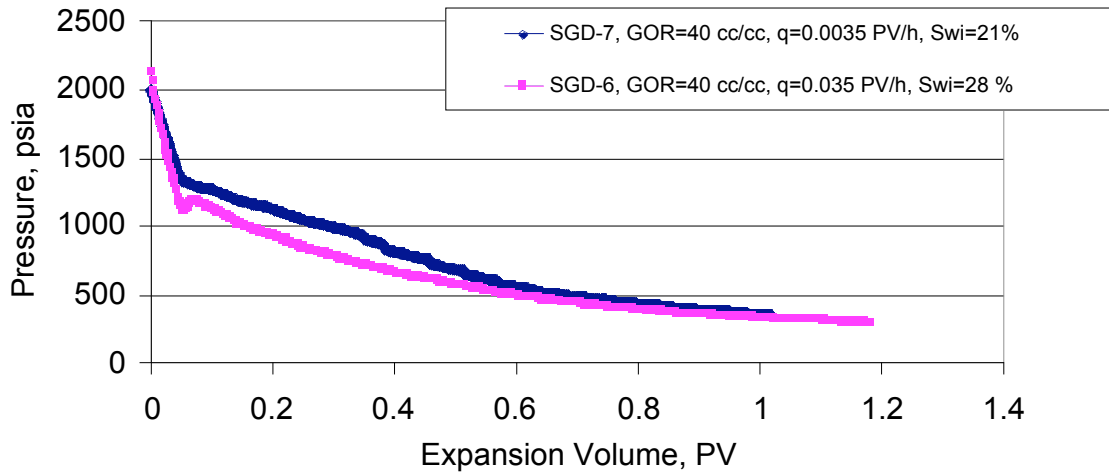


Figure 5. Pressure history of primary heavy oil recovery for West Sak crude oil in the presence and absence of initial water saturation.

The results in Fig. 5 do not display significant difference from one another despite the large variation in depletion rate. With the exception of the small apparent supersaturation in the depletion at rate of 0.035 PV/hr, dynamic results are roughly identical and display little rate-dependent effects.

The recovery versus pore volume expansion for all tests performed is reported in Fig. 6. The initial solution gas-oil ratio, initial water saturation, and depletion rate are all varied independently. The striking feature of Fig. 6 is the lack of sensitivity to experimental conditions because in all cases, the ultimate recovery is about 22-23% of the original oil in place (OOIP). Some differences in the dynamics are noticed. For instance, the test with the solution GOR of 40 in the presence of a roughly 30% initial water saturation at a low depletion rate produces oil the most rapidly with respect to the expansion volume. Differences in the initial recovery are relatively minor across all of the cases.

The evolution of the effluent bubble texture was measured for these new depletion experiments. Recall, the visualization cell at the sandpack outlet in Fig. 3. Figure 7 presents a typical set of images. Gas first appears at the outlet at an average sandpack pressure of 1337 psi, near the solution bubble point. As pressure declines, the features of the flowing gas increase in size. It is apparent that the gas produced is not bubbly or foamy in nature.

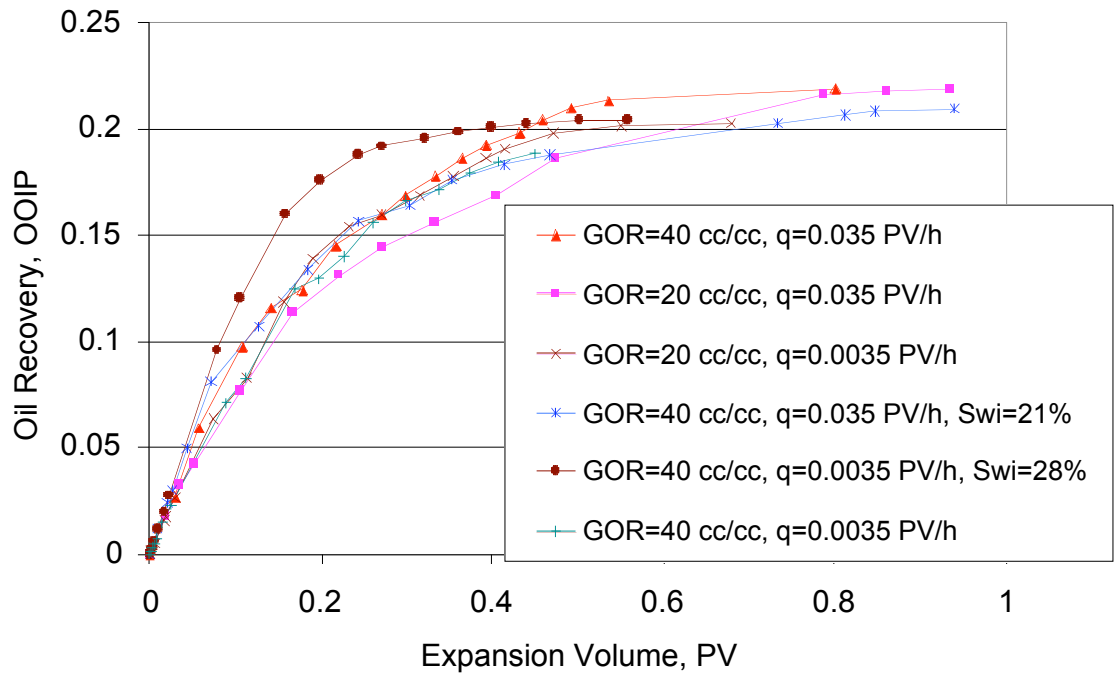


Figure 6. Summary of oil recovery history for depletion of viscous West Sak oil in representative sandpicks. Unless otherwise noted, the initial water saturation is zero.

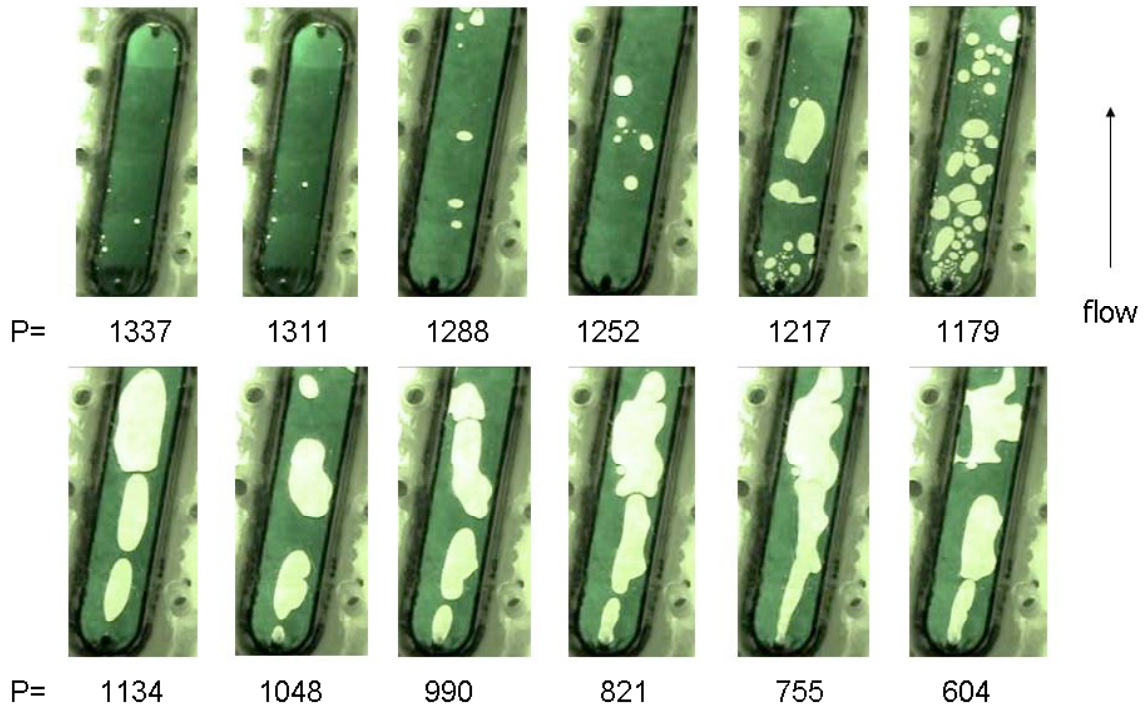


Figure 7. Flowing gas bubble behavior of West Sak crude in visual cell – (0.035 PV/hr, SGOR=40), P in psi.

In summary, the following factors have been observed for pressure depletion of West Sak Crude oil: (1) recovery is relatively insensitive to depletion rate if viscous oil does not foam, (2) solution gas-oil ratio is important to final recovery, (3) initial water saturation does not appear to change the ultimate oil recovery, (4) gravity has a positive effect on recovery of both oil and gas, and (5) in all cases, primary recovery in the laboratory was greater than 20% of the OOIP.

1.2 Cold Production– Simulation of Cold Production

This subtask was not pursued due to reduced project effort.

2.1 Thermal Recovery– Review of advanced well completions

An addendum to our report for the period October 1, 2004 to March 31, 2005 (Kovscek and Castanier, 2005) summarizes our findings. Briefly, over the past 30 years, very little significant change is described relevant to drilling or producing wells in the permafrost environment. Despite the preponderance of descriptions of vacuum insulated tubing, it is likely not the insulating method of choice due to the difficulty of obtaining low heat loss at the coupling between sections of tubing. New insulation techniques and materials are described in the literature for steam injection wells and offshore applications. With this technology it should be possible to produce using thermal methods the currently nonexploited heavy-oil resources of Alaska such as Ugnu or West Sak. No commercially available products were found.

In a project separate from this, the properties of aerogel insulations were evaluated and found to have exceptionally low thermal conductivity. A model of heat transfer from hot insulated tubing to cold permafrost indicated that these aerogel insulations had great potential to protect the permafrost against melting (Marques, 2007). Hence, new well designs and insulating materials have the potential to open cold environments to thermal recovery operations.

2.2 Thermal Recovery– Thermal Gravity Drainage

When viewed solely from a reservoir perspective, thermally enhanced oil production, and most likely steam injection, is clearly the option to employ for most heavy oils. Heating reduces oil viscosity substantially thereby improving flow rates and speeding up ultimate recovery. Two studies were conducted in this subtask. The first was an analytical model for cyclic steam injection of a horizontal well. The second was a scoping study of the effect of heterogeneities on the steam-assisted gravity drainage (SAGD) process.

Cyclic Steam Injection

A new model was synthesized based on established models for cyclic steam injection in vertical wells. In the reservoir, steam is introduced near the bottom of the formation through a horizontal well, displaces the oil and rises to the top of the formation where it is trapped if an impermeable cap rock exists. The shape of the steam zone is, therefore, assumed to be triangular. Steam heats the colder oil sand near the condensation surface. During production oil drains along the condensation surface by a combination of gravity and pressure difference in the production well as does steam condensate (Aziz and Gontijo, 1984). In addition, oil drains through the steam chamber into the production well. The mechanisms involved in oil production during cyclic steam injection are diverse and intricate. Reduction of oil viscosity as a result of an increase in the temperature greatly improves the production response. Gravity drainage and pressure

drawdown are the major mechanisms of oil production in the case of cyclic steaming. Heat losses from the reservoir to the overburden are computed with a variation of the approach proposed by Myhill and Stegemeier (1978). The semianalytical model is verified by comparing results with those obtained from a commercial, thermal, reservoir simulator.

The analytical model is based on the development of a triangular steam zone, in vertical cross section, as shown in Fig 8. Steam is introduced near the bottom of the formation through a horizontal well, displaces the oil and rises to the top of the formation where it is trapped beneath the reservoir cap rock. Steam heats the colder oil sand near the condensation surface of the triangular shaped steam zone. During production, oil drains along the condensation surface and throughout the steam chamber due to a combination of gravity and pressure difference in the production well. Steam condensate drains similarly. The primary assumptions are that the steam-zone adopts a triangular shape, steam injection rate is constant, heat losses are described analytically, and oil production occurs due to a combination of gravity forces and pressure drop.

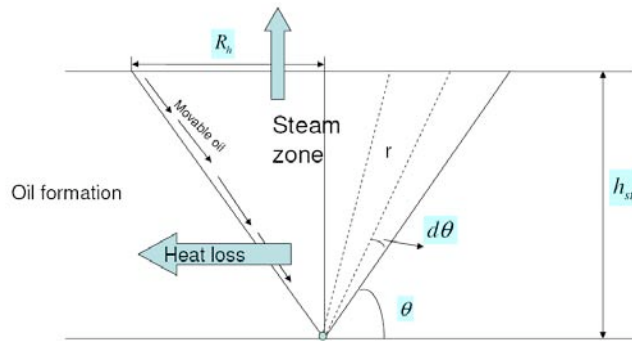


Figure 8. Schematic triangular steam-zone geometry.

The model is divided into three parts in accordance with three periods: the injection period, the soaking period, and the production period. Appropriate physical equations are developed for each period. Full details are available in the M.S. report of Liang (2005). The analytical model is validated by comparing results with a thermal reservoir simulator STARS. The data used to test the model are initially from the work of Elliot and Kovscek (2001) on application of single well steam assisted gravity drainage to heavy oil. The simulation results reported here are new, however.

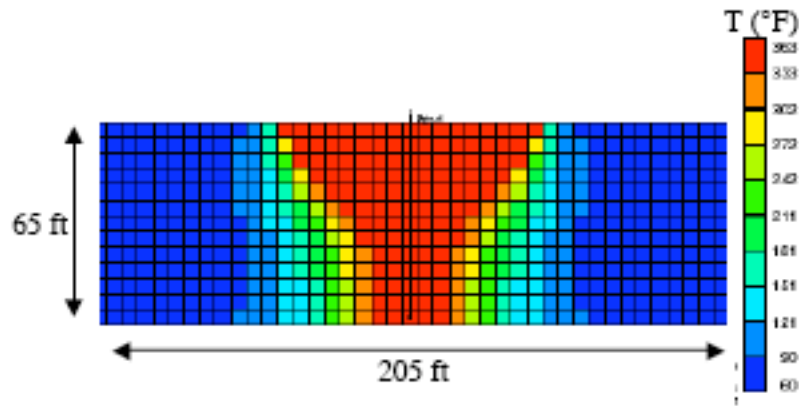


Figure 9. Triangular heated-zone geometry computed by STARS.

Several comparisons have been made to illustrate the accuracy of the analytical model. Sample results are displayed in Figs. 9 to 12. Figure 9 illustrates a temperature profile as obtained by thermal reservoir simulation. The production well is located at the base of the triangular shaped steam zone. Three cycles of steam injection have occurred over the course of roughly a year. The temperature in the red-shaded region above the well is about 360 °F whereas the initial reservoir temperature, shown in blue, is about 60 °F. Figure 9, thus, indicates a triangular shaped steam zone, as we assume in our model, Fig. 8. The comparisons between the model and STARS are computed based on identical cumulative heat injection. Further comparisons were made among oil rate, cumulative oil production, and cumulative water production, Figs. 10 to 12. Both the cumulative oil and the cumulative water production match well with STARS, Figs. 11 and 12. There is some discrepancy in the agreement of oil rate versus time, Fig. 10, between the two methods. STARS produces a greater peak oil rate at the beginning of the production followed by some small oscillations in rate. Overall, agreement among analytical and numerical reservoir simulation results are in agreement and favorable.

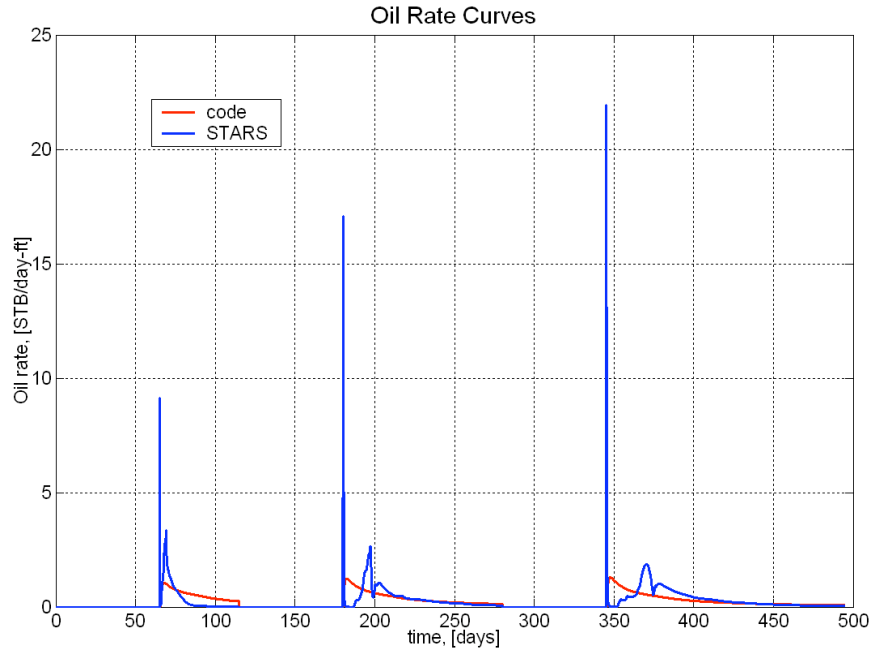


Figure 10. Oil rate predictions for cyclic steaming. Comparison between semianalytical theory (code) and numerical reservoir simulation (STARS) results.

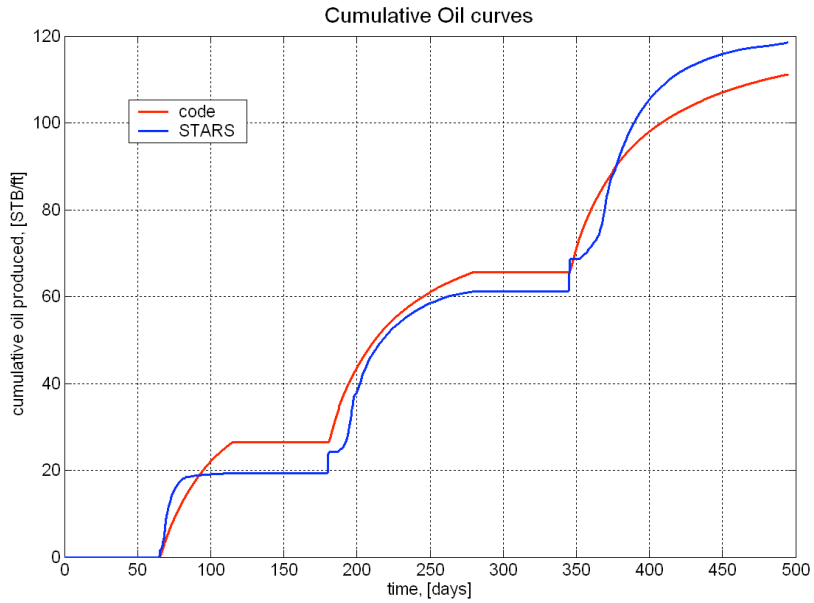


Figure 11. Cumulative oil predictions for cyclic steaming. Comparison between semianalytical theory (code) and numerical reservoir simulation (STARS) results.

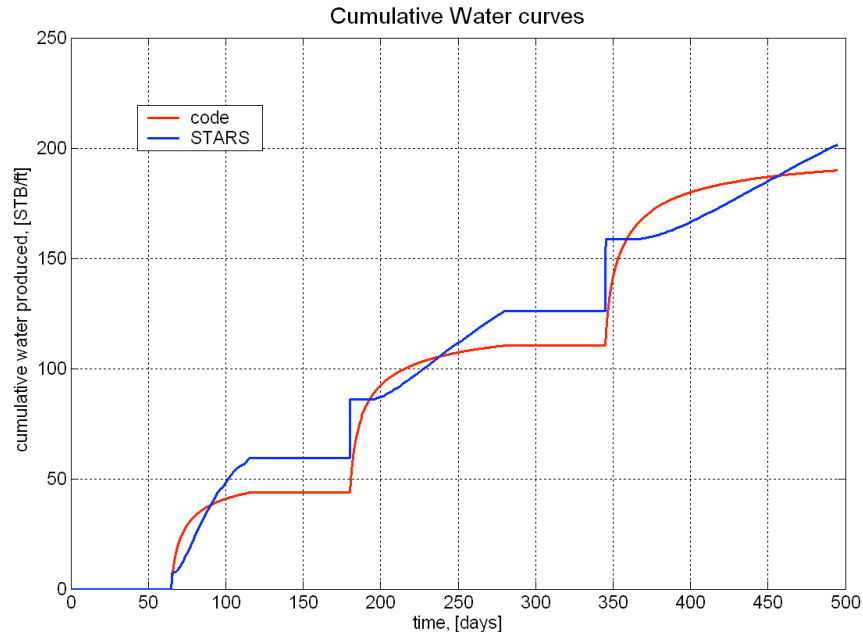


Figure 12. Cumulative water predictions for cyclic steaming. Comparison between semianalytical theory (code) and numerical reservoir simulation (STARS) results.

SAGD

SAGD is a promising approach for recovering heavy and viscous oil resources and could follow cyclic steam injection. This approach ensures a stable steam displacement front by applying gravity as the only driving force and allows an economical oil rate by using horizontal wells. In the SAGD process, steam is injected continuously into the reservoir via the upper well of the two parallel wells placed one above the other at a short vertical distance of about 5m. Heated oil and condensed water drain downward by gravity and are produced through the lower well. The success of this process is demonstrated by both field and laboratory studies, most of them based on homogeneous reservoir models. Nevertheless, a comprehensive understanding of the effects of reservoir heterogeneities on SAGD performance is required for the practical implementation of SAGD.

This work presents a numerical investigation of the effects of reservoir heterogeneities on SAGD using a stochastic model of shale distribution. Two flow regions, the near well region (NWR) and the above well region (AWR), are identified to decouple the complex effects of reservoir heterogeneities on the SAGD process. Numerical simulations were conducted with a number of realizations to compare SAGD performance in terms of the effects of NWR and AWR. Hydraulic fracturing is proposed to enhance steam chamber developments for reservoirs with poor vertical communication and the feasibility of hydraulic fracturing is discussed in terms of in-situ stress and well orientations.

A synthetic reservoir was created representing a generic, shallow, heavy-oil reservoir. The reservoir is approximately 300m deep with a pay zone thickness of 20m. The reservoir parameters are taken from typical data used in the literature for studies of the oil sand deposit of Alberta, because they are readily available. These are, perhaps, similar characteristic of the more viscous, heavy, and shallow North Slope resources. Initial oil and water saturations in the pay

zone are 0.8 and 0.2, respectively, and reservoir temperature is 10 °C. The reservoir formation consists of clean sands and shaly sands that contain laterally-orientated thin shale. The absolute permeability in clean sands is 3,000 mD in the horizontal direction and 1,800~mD in the vertical direction. The representation of shale in the model is described in detail shortly. Both clean sands and shaly sands have a porosity of 32%. Water-oil and gas-oil relative permeability curves used in this study are depicted together with the oil temperature versus viscosity curve in Fig 13.

A horizontal production well with a length of 1000m is placed 1.5m above the bottom of the pay zone. A horizontal injection well with the same length is drilled parallel to the producers with a vertical well spacing of 4m. The horizontal spacing between well pairs is 100m. A confined formation unit with one well pair in the center is considered, assuming symmetry between well pairs. This grid contains 67 grid blocks each 1.5m wide in the horizontal (x) direction except that the center column is 1.0m and 20 grid blocks each 1.0m thick in the vertical (z) direction. The fine grid size in the vertical cross section provides high resolution capable of mimicking complex flows occurring mainly in the vertical plane in the SAGD process. The three-dimensional model is specially designed to compare the effect of fractures. To achieve enough spatial resolution in all the three dimensions while to limit the total number of grid blocks for reasonable machine run time, non-uniform grids of 37 by 37 by 20 are adopted in this 3D model.

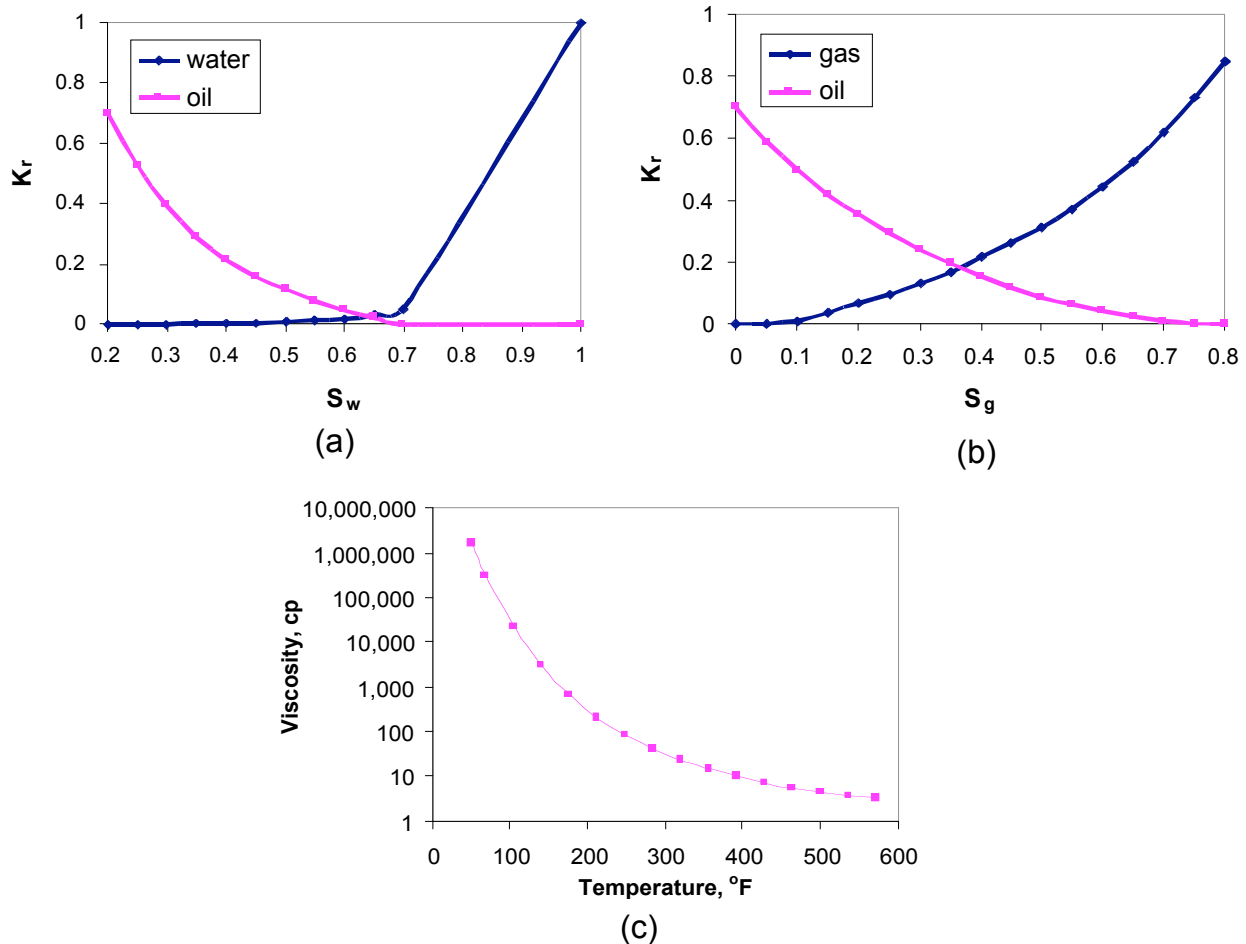


Figure 13. Relative permeability and viscosity versus temperature relationship for hypothetical reservoir.

Shale Distribution

Reservoir heterogeneity is introduced by including randomly-distributed thin shale. The shale is characterized by extremely low vertical permeability, typically in the range of 10^{-6} to 10^{-3} mD. For laterally-oriented thin shale, it is acceptable to assume that the occurrence of shale in sand reduces dramatically the vertical permeability of the sand block, but has no effect on the horizontal permeability. Therefore, a reduction factor of 10^{-5} is applied to the vertical permeability of the shaly sand blocks in this study. Given the fact that it would be impractical to obtain exact geological information of sand and shale sequences, we model the distribution of shaly sands with a stochastic representation based on a geostatistical method, sequential indicator simulation (SISIM). In the geostatistical model, the probability of the shaly-sand occurrence P_s and correlation length of shale L_s are the two key parameters that determine the fraction of shaly sands and the continuity of shale in the distribution, respectively. These two characteristics of shale distribution, as demonstrated later, play important roles in the SAGD process. For each pair of P_s and L_s , SISIM generates a number of realizations, all honoring the predetermined data (e.g., hard data) and, thus all being equally probable. Figure 14 shows one of the realizations obtained with $P_s = 30\%$ and $L_s = 1\text{m}$ in both two (vertical cross section) and three dimensions.

Representation of Fracture

Another common cause of reservoir heterogeneity is the presence of fractures, either naturally-existing or hydraulically-induced, that have very high permeability and very small pore-volume. In this study, we only consider hydraulic fractures. The effect of a hydraulic fracture on the petrophysical properties of the sand block where it is located is approximated as follows. A fracture permeability of 10^6 mD and fracture opening of 0.01 m are assumed. The absolute permeability in the direction perpendicular to the fracture plane remains unchanged. For the directions parallel to the fracture plane, the permeability of the grid block is changed to the equivalent permeability computed by arithmetic averaging according to the fracture and block geometries.

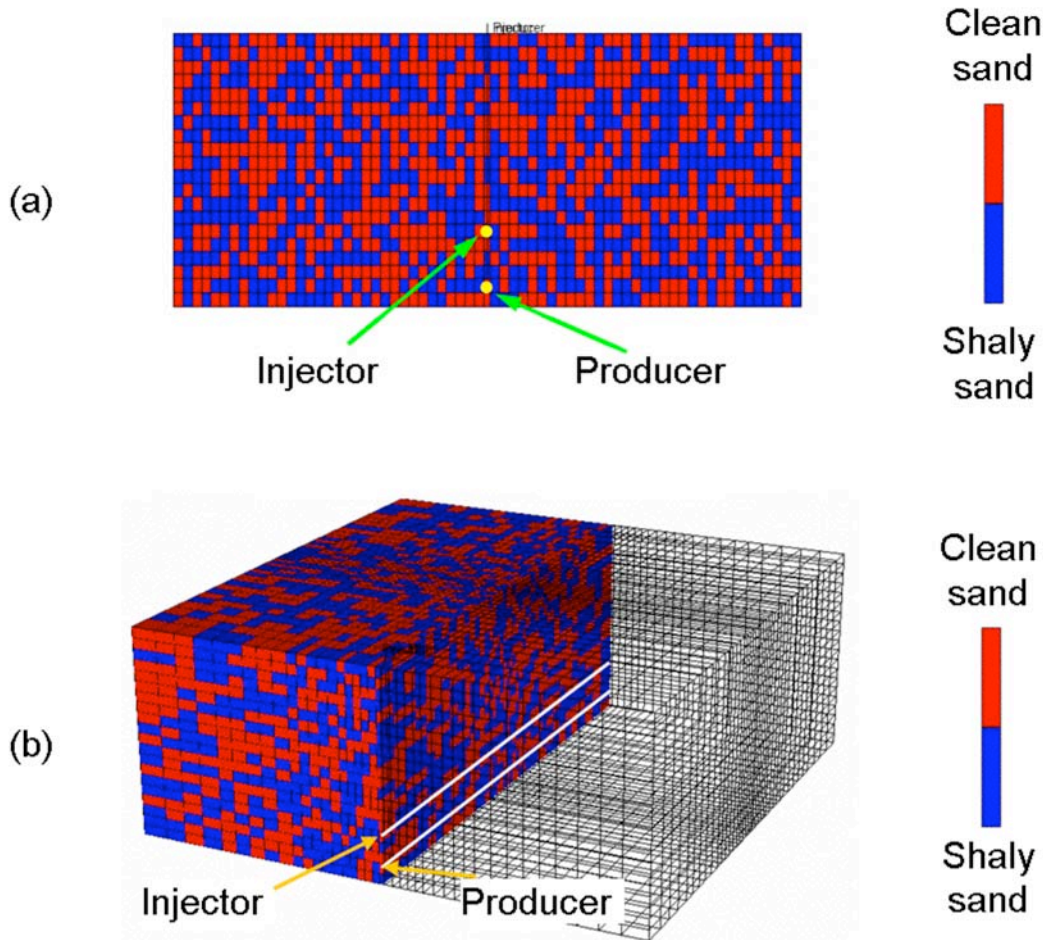


Figure 14. Numerical grids for SAGD simulation (a) 2D model and (b) 3D model.

Simulation Runs

The thermal, compositional simulator model, STARS was used for all the simulation runs. These simulation runs are classified into three groups: (1) varying NWR, (2) varying AWR, and (3) induced hydraulic fractures. For the baseline simulation runs, electrical conductive preheating is first carried out at both well locations for 90 days to mobilize the oil around wells and to establish hydraulic communication between the two wells. Then 95% quality steam at 435 psi (i.e., 15 psi greater than the initial pay zone pressure) is injected continuously at the upper well. The lower production well is operated with steam trap conditions to avoid excessive steam production. This steam trap control is achieved in the simulation by setting production temperature 18°F below steam temperature and establishing a liquid leg above the producer (Edmunds, 1998; Egermann 2001). The simulation runs are terminated after 10 years of production.

Results–Shales

Two sets of simulation runs were conducted to investigate the effect of AWR in terms of shale percentage and shale continuity. In the first set, the fraction of shaly sands is fixed to 30%, and the shale correlation length is varied from 1 m, to 4 m, 8 m, and 16 m to generate three equal-probable realizations. In the second set, the shale correlation length is fixed at 4 m, and the

fraction of shaly sands is changed from 10% to 30% and 50%. All the realizations are conditioned to the same pre-determined NWR data shown in Figure 14.

Figure 15 compares the effect of shale continuity in the AWR on SAGD performance. For each case, reservoir simulation runs were conducted with three realizations, and one of them is plotted in the figure as their responses are consistent. It is seen that the oil production is strongly correlated to the shale continuity. The oil production rate curve for the more continuous shale, for example, is below that for the shale with shorter correlation length. As the shale becomes more continuous, from 1 m to 16 m, the oil recovery factor decreases from 70% to 23% and the cumulative oil steam ratio reduces from 0.3 to 0.15. Notice that this decreasing trend is not uniform. For the change in shale continuity when its correlation is short, e.g., from 1m to 4m, the resulting difference in the SAGD performance is not obvious; but when the shale correlation length becomes larger, such changes cause dramatic reduction in oil production. This is because the steam chamber expansion mainly occurs in the AWR. The flows associated with the steam chamber expansion are of relatively long characteristic length depending on the steam chamber height. As a result, the horizontal barrier formed by shale only affects the steam chamber development when it is quite long. Otherwise, steam easily bypasses the discontinuous shale and extends the chamber further into the un-touched zones.

The comparison in Fig. 15 indicates that shaly sand with correlation length greater than 8 m impairs SAGD performance substantially. This critical value is just about half of the formation thickness. Such results confirm our analysis of the flow characteristic length.

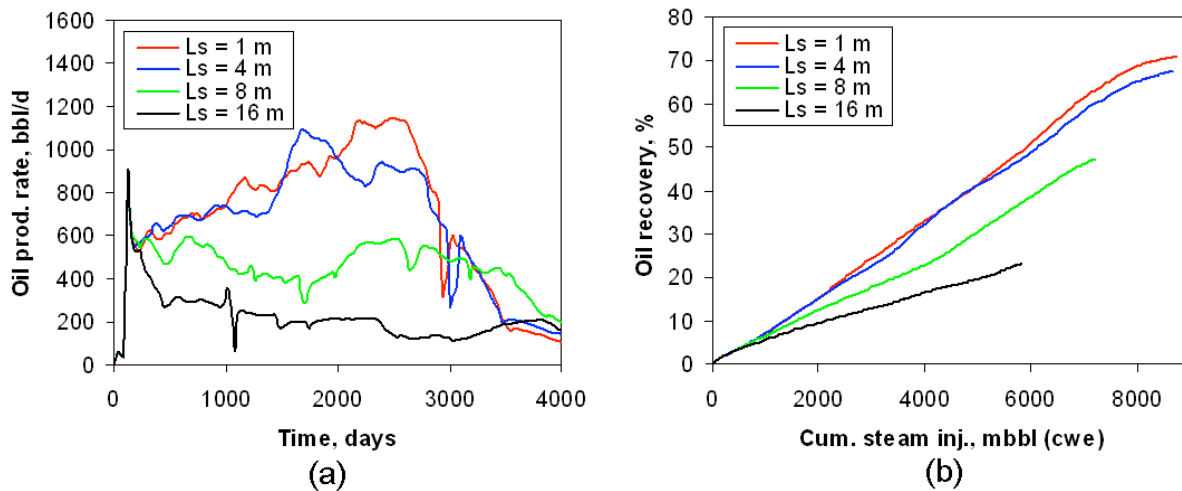


Figure 15. Effect of correlation length of shaly-sand in AWR on SAGD performance. (a) oil production rate and (b) oil recovery versus cumulative steam injection.

Hydraulically Fractured Injectors

Hydraulically-induced fractures always propagate perpendicular to the least principal stress (Hubbert and Willis, 1957). Therefore, to determine the orientation of hydraulic fractures, the tectonic stresses in a reservoir should be analyzed to obtain the knowledge of the least principal stress. The orientation of S_{Hmax} is determined from the borehole breakout analysis of vertical wells. In general, within formations shallower than about 150m, the vertical stress corresponds to

the least principal stress. Beyond a depth of roughly 200 m, the least principal stress changes to the minimum horizontal stress. This observation indicates that the orientation of hydraulic fractures correlates with depth.

Consequently, we consider two categories of SAGD projects according to the formation depth: shallow SAGD and deep SAGD. In a shallow SAGD project, the least principal stress corresponds to the overburden stress. Once a fracture is induced hydraulically, the dominant orientation of the fracture plane is horizontal, Fig 16(a). For deep SAGD projects, the reservoirs have a minimum horizontal stress corresponding to the least principal stress. The dominant orientation of the induced fracture plane is vertical. In addition, depending on the drilling direction of the horizontal well pairs in a SAGD process, a vertical fracture can be parallel or perpendicular to the wells, Figs 16(b) and (c). In the following subsection, we examine the effects of the fractures with three different orientations on the SAGD process by reservoir simulation.

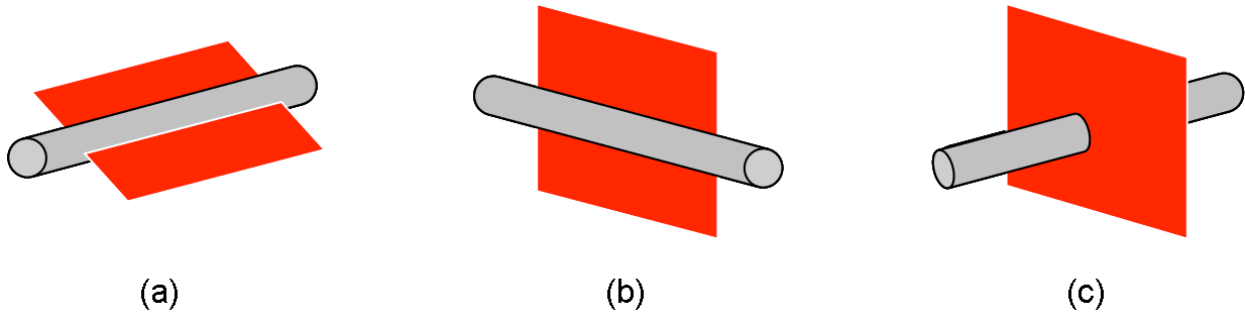


Figure 16. Schematic of possible orientations of hydraulic fractures (a) horizontal fracture, (b) vertical fracture parallel to, and (c) vertical fracture perpendicular to well.

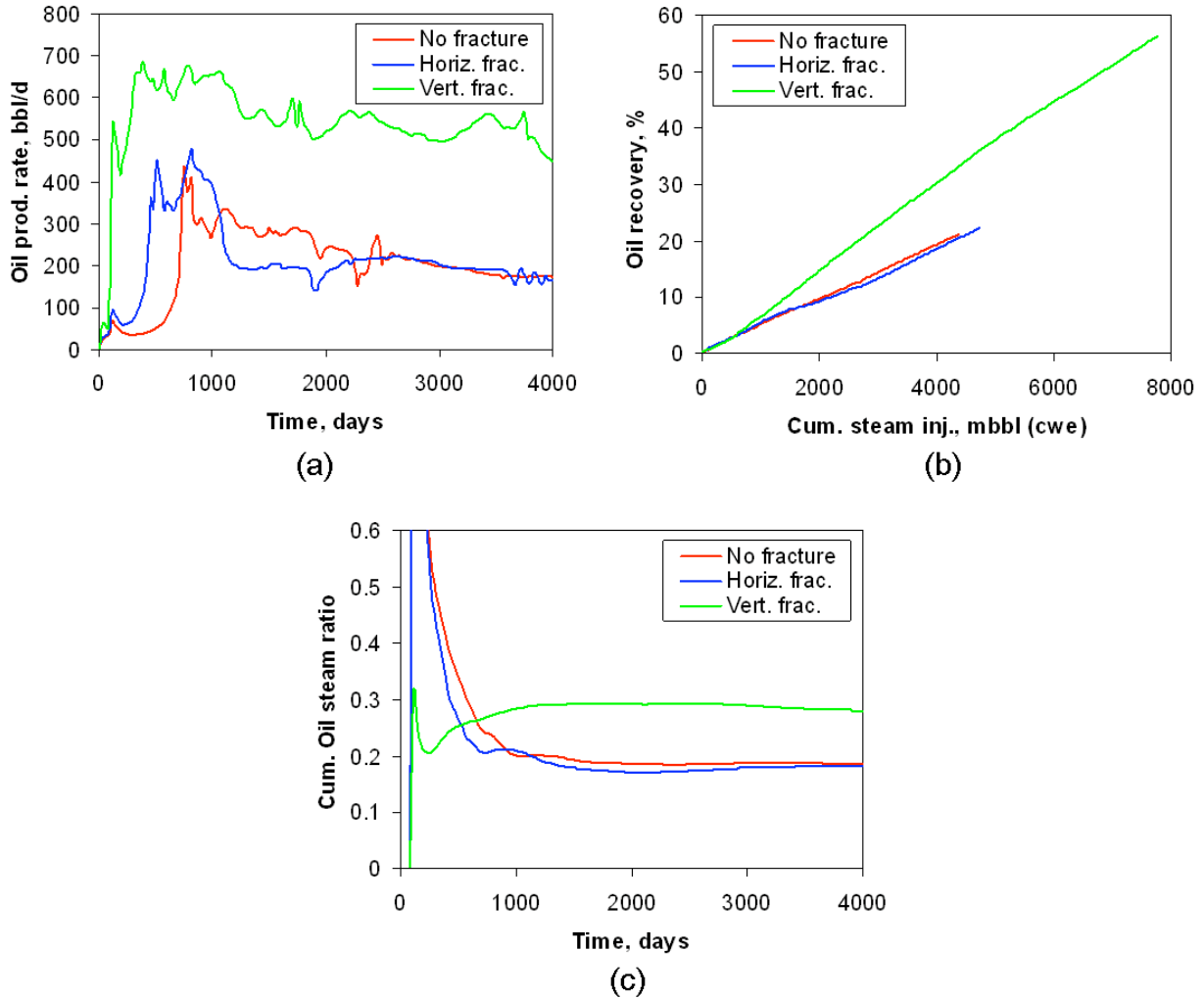


Figure 17. Comparison of no fracture, horizontal, and vertical fractures. (a) oil production rate, (b) oil recovery versus cumulative steam injection, and (c) cumulative oil-steam ratio.

Figure 17 compares SAGD performances of the three shale/fracture configurations. The three cases share the same shale distribution that has 50% shale and shale correlation length of 1m. In the base case (red curve), the oil production rate starts with a low value and then experiences a jump at about 700 days that leads to the main production period. The oil production rate, after reaching a peak, drops back to 300 bbl/d, and remains at a plateau rate with a slow decline for the rest of the production time. The final oil recovery is only 24% and the cumulative oil steam ratio is 0.2. For the case with horizontal fractures, the curve (in blue) of oil production rate shows a similar shape as the base case except that the main production period occurs 300 days earlier. For the case with a vertical fracture, the main oil production period starts shortly after steam injection and exhibits a much greater average oil rate, more than twice the oil rates of the other two cases. As seen in Fig 17(b), the base case yields an oil recovery of only 21%. Adding horizontal fractures increases the oil recovery to 24%, while the presence of the vertical fracture improves the oil recovery dramatically, to 56%.

The observed differences among various horizontal and vertical fractures are explained by examining how the steam chamber profile is affected by the presence of fractures. Figure 18 shows the temperature profiles in the vertical cross section of the formation after 3 years of steam injection. Because of shaly sands and resulting very low vertical permeability, the steam chamber in the base case develops very little in the formation after 3 years of steam injection. Compared with the base case, the horizontal fractures illustrated in Figure 13(b) help the steam chamber extend laterally to a greater extent. Little improvement in the vertical direction is found.

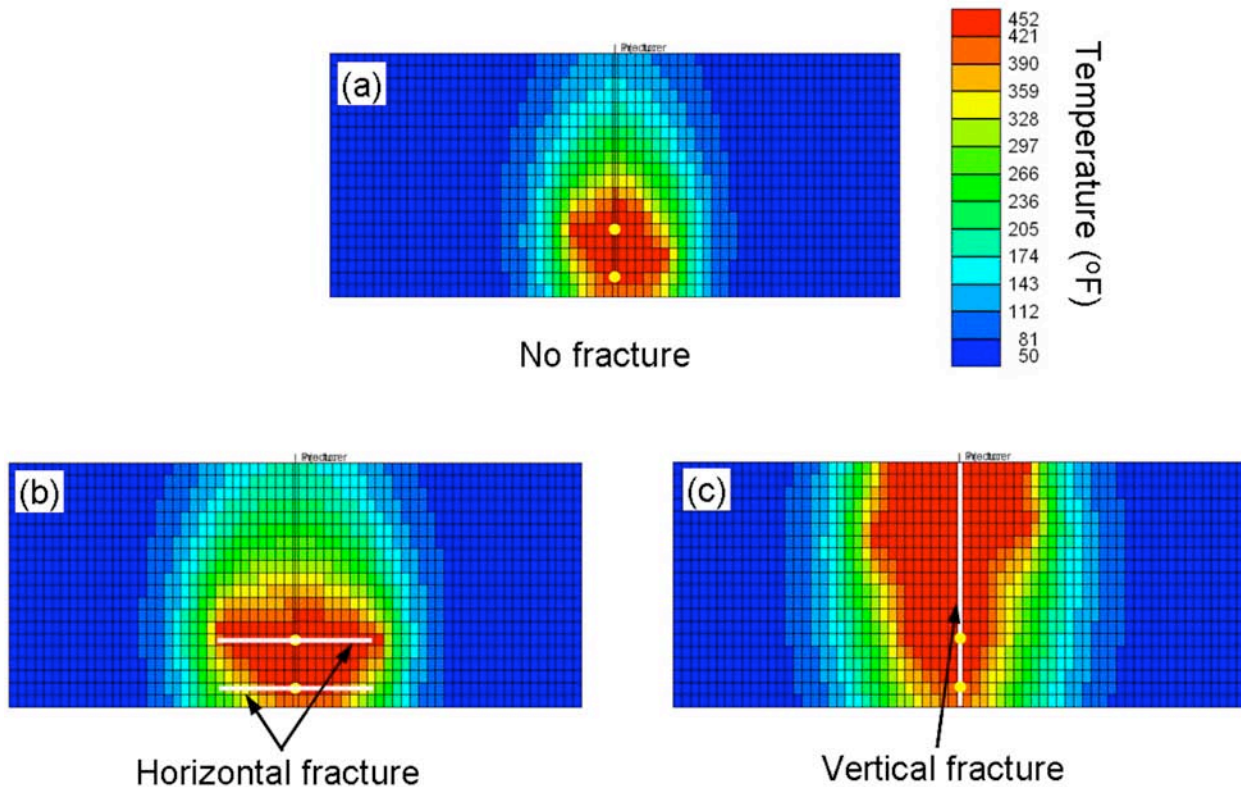


Figure 18. Temperature profiles after 3 years of steam injection. (a) no fracture, (b) horizontal fracture, and (c) vertical fracture.

The steam chamber in the case with a vertical fracture, however, is developed fully through the whole thickness of the formation. This is because the presence of a vertical fracture provides a highly permeable vertical path for steam, that substantially improves the vertical development of the steam chamber. According to Butler's analytical theory, the oil drainage rate is proportional to the square root of the chamber height. Hence, the improvement in the vertical development of the steam chamber accelerates oil drainage. Consequently, the performance of SAGD is enhanced dramatically. As can be seen in Fig. 18, the volume of a steam chamber connected to a vertical fracture is much larger than the other two cases.

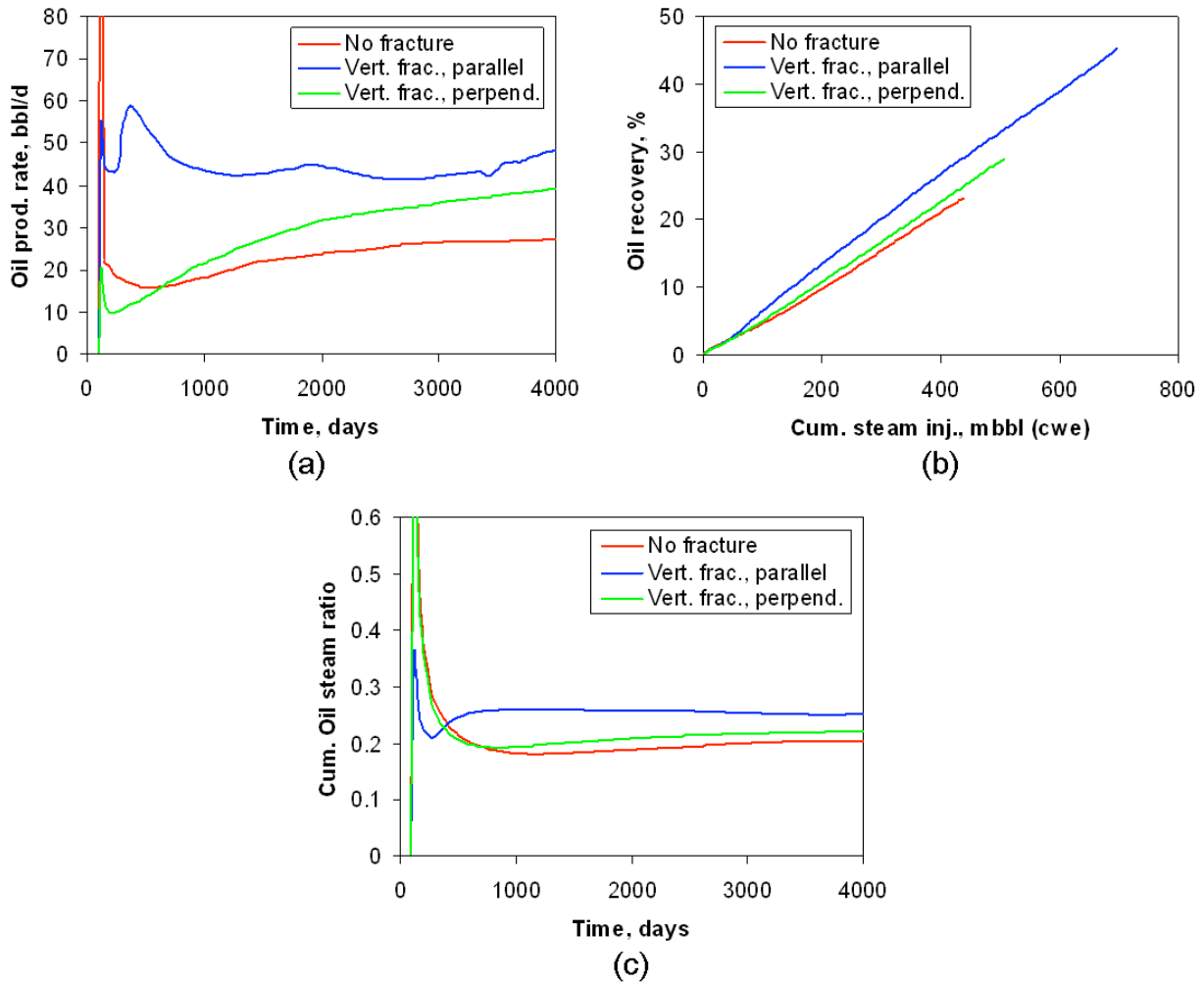


Figure 19. Comparison of formation with/without vertical fractures. (a) oil production rate, (b) oil recovery versus cumulative steam injection, and (c) cumulative oil-steam ratio.

The vertical fracture considered above is along the direction of the well. Another orientation of a vertical fracture is perpendicular to the well if the well is drilled along the direction of the minimum horizontal stress. The effects of these two situations are investigated with the three-dimensional grid system Fig 14. Similar to the 2-D model, we consider three cases: a base case with no fracture and two cases with a vertical fracture oriented parallel to the well and with a vertical fracture perpendicular to the well, respectively. Figure 19 compares the predicted oil production for the three cases. As can be seen in Fig 19(a), the case with the vertical fracture along the wells gives the oil production rate more than two times that of the base case. It is interesting that when a vertical fracture perpendicular to the well exists, the oil production starts with a lower rate than the base case and then catches up and exceeds the latter in the late stage. This is explained as follows. In the operation of SAGD, we set the steam trap control to avoid direct steam production. The vertical fracture perpendicular to the well creates a very permeable channel between the two wells at the perpendicular intersection plane. This actually increases the heterogeneity contrast along the wells. To avoid steam breakthrough, the steam trap control has to set a low steam injection rate at the beginning because of high injectivity contrast along

the well. As a result, the oil production rate is low during the early stage of production. When the steam chamber develops more around the wells, the injectivity contrast along the well is smoothed out and then steam is injected at the reservoir's full capability during late stages. Because the vertical fracture, as demonstrated in the 2-D model, helps the vertical development of a steam chamber, oil production shows an increase in the late time. Fig. 19b shows that the oil recovery factors are 23%, 29%, and 45% for three cases.

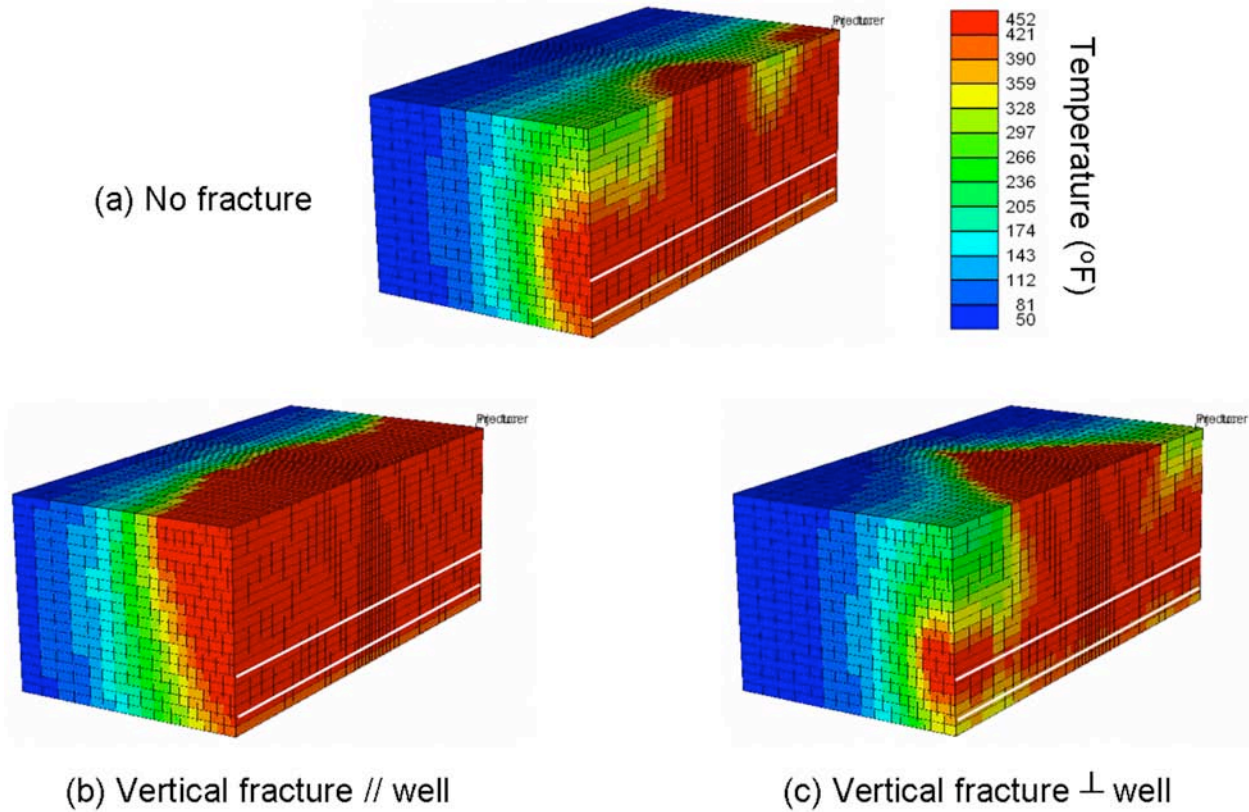


Figure 20. Temperature profiles after 6 years of steam injection.

Figure 20 shows the steam chamber profiles after 6 years of steam injection in the three cases. As expected, in the case with a vertical fracture along the well, Fig. 20 (b) the steam chamber is well developed and a large volume of the reservoir is swept by steam. For the case with a vertical fracture perpendicular to the well, Fig. 20(c), steam extends along the fracture plane to the top of the formation and forms a nice chamber. As can be seen, the well-developed steam chamber is limited only near the fracture plane. In the regions around the two ends of well, the development of the steam chamber is very poor. This means that the improvement of the vertical fracture perpendicular to the well direction is moderate. Note that this result is obtained with the assumption of one vertical fracture perpendicular to the well within the interval of interest. It is possible to induce hydraulically multiple fractures that likely result in successful steam chamber development along the whole length of well and promote oil production considerably.

The above simulation results suggest that vertical fractures enhance the SAGD process. The real challenge of such an idea is the feasibility of generating the desired vertical fractures in the field and obtaining effective steam trap control. To achieve vertical fractures propagating along the well, it is required that the horizontal wells be drilled along the direction of the maximum horizontal stress S_{Hmax} . This requirement, fortunately, coincides with the general field practice that horizontal wells are normally drilled exactly in such a way to ensure well stability. If the well stability is not an issue (e.g., strong rock) for a particular reservoir, drilling the well pair along S_{Hmin} and creating a series of vertical fractures perpendicular to the well direction may provide an alternative to enhance the performance of the SAGD process.

2.3 Thermal Recovery– Comparison of cyclic steam injection and downhole heating

This subtask screens a series of technically feasible methods for recovering heavy oil from Alaska North Slope reservoirs and benchmarks them versus cyclic steam injection. A pattern simulation approach is employed to understand the benefits and drawbacks of various recovery methods for viscous oil. The options screened make use of horizontal wells chiefly because such wells give maximum contact of the well with the reservoir when the reservoir is fairly continuous. Additionally, subtask 2 demonstrated the advantage of horizontal wells even if the formation was significantly heterogeneous in the vertical direction. The options include: (1) cyclic steam injection, (2) continuous steam injection to achieve a thermal gravity drainage process, (3) electrical heating via a heating element placed horizontally within the reservoir, and (4) miscible gas injection in a VAPEX fashion (Butler and Mokrys, 1991). These options were explored using an appropriate thermal reservoir simulator (i.e., CMG STARS) with the ability to include noncondensable gas components. All options were evaluated using a common reservoir model.

Generally, results indicate that electrothermal, conventional steam-based, and thermal gravity drainage enhanced oil recovery techniques all appear to be applicable to “prime” Ugnu reservoir conditions to the extent that reservoir architecture and fluid conditions are modeled faithfully in the representative 2D vertical section employed here. The model presents favorable recovery characteristics such as oil that is mobile at initial reservoir temperature, moderate solution gas-oil ratio, and an average permeability of roughly 400 md. These characteristics aid recovery of this viscous oil. The relatively high initial reservoir pressure proved difficult to deplete and led, consequently, to moderately high injection pressures and temperatures for steam. The extent of reservoir layering and vertical communication are further important factors affecting recovery.

While steam injection and the gravity drainage process are fairly well known, the particular type of electrical heating studied here needs further description. Electrical heating using mineral insulated (MI) cables (Afkampur, 1985) placed in a wellbore is, perhaps, the most conceptually simple thermal recovery process. The heating element is installed in the production well or in a gravity drainage fashion with the heater positioned above the producer. In electrical-heating-assisted recovery, electrical heaters are introduced in the formation. Alternating current flows along the heaters, but not through the formation. The temperature of the heaters increases and then heats the oil around them. Description of the history and principles of this method is found in the literature (Rangel-German et al, 2004). This type of electrical heating method does not require surface or down hole steam generation, potentially allows differential heating in the horizontal direction, and does not suffer from steam breakthrough from the injector to the producer. Potentially, there are significant capital cost savings as costly steam generation and hot

fluid handling facilities are obviated. For all of the successes and potential of cyclic steam injection, steam drive and SAGD, heat loss from the formation to the under and overburden is still a concern. The application of electrical-heating-assisted recovery was motivated by the advantages mentioned above and the premise that energy could be saved by reducing heat loss in the surface facilities and along the well bore in comparison to steam injection.

Model Description

Basic rock and reservoir properties that were selected as representative are shown in Table 2. In our simulation, several models of the distribution of permeability and porosity were created. All are 2D grid models. In addition to the model describing the porosity and absolute permeability of the reservoir, a fluid model describing the reservoir fluid components and properties, and relative permeability models were developed for the simulations. Details follow.

Grid definition: The grid is a 2D vertical model of size 1 by 39 by 19 grid blocks, representing a 1 ft by 525 ft by 95 ft volume section of the reservoir. The dimensions of the grid blocks were $\Delta y = 93.5, 46.6, 7*10, 21*5, 7*10, 46.6, 93.5$ ft for 525 ft (160 m) total, and $\Delta z = 19*5$ ft for 95 ft (29m) total.

Table 1: Rock and reservoir properties

Porosity	0.33
Permeability	762 mD
Initial pressure	1300 psi
Initial temperature	57.92 °F
Initial oil saturation	0.6
Initial water saturation	0.4
API	14.6
Efficient formation compressibility	$5*10^{-4}$ Btu/ft ³ -F

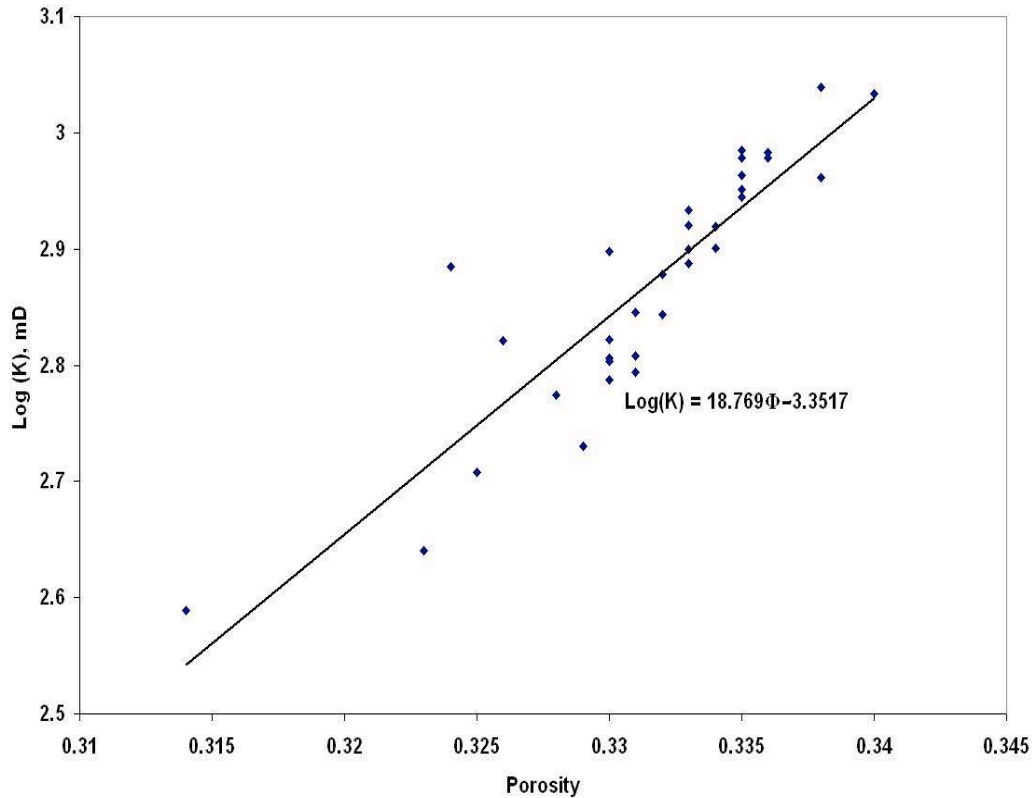


Figure 21. Correlation of permeability and porosity for reservoir sands.

Reservoir model: Representative permeability and porosity data from the Ugnu reservoir were provided by Industrial Partners. The permeability in the sample data is in the range of 388 mD to 1094 mD, with an average of 762 mD. The porosity in the sample data is in the range of 0.314 to 0.34, with an average of 0.33. The logarithm of permeability is correlated with porosity as shown in Figure 21. Using the histogram of the field data, several permeability and porosity realizations were created using sequential Gaussian simulation. Figure 22 shows a realization of the heterogeneous distribution of permeability and porosity without continuity in any direction and a realization of heterogeneous permeability and porosity distribution with great continuity in the horizontal direction (correlation ratio 1000000:1). After obtaining porosity and permeability realizations, the reservoir simulation grid model was populated with these porosity and permeability data. For the homogeneous cases, the whole grid was assigned a uniform porosity (0.33) and permeability (762 mD).

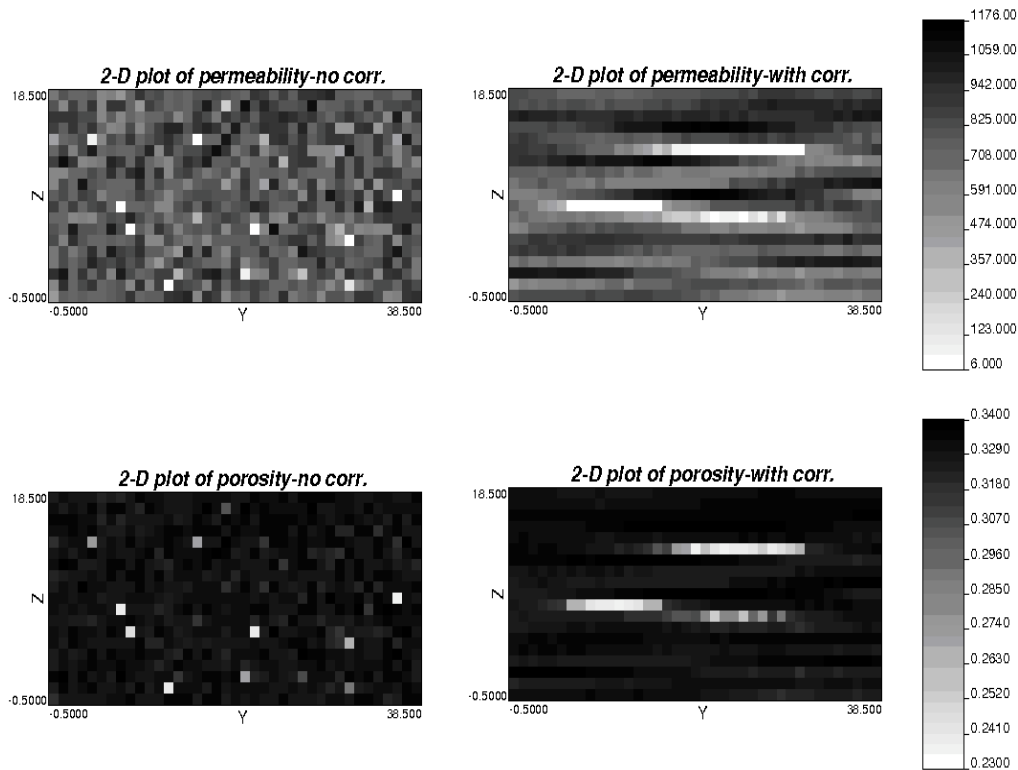


Figure 22. Realizations of the distribution of reservoir heterogeneity by varying the correlation length.

Fluid model: The reservoir fluid is represented as a six-component model (water, four oil components and solvent). A multi-component fluid analysis of the component properties of Schrader Bluff crude oil (Guler et al, 2001) was used to construct the 4 representative oil-phase components. The component compositions were adjusted to give a greater fraction of heavy components and thereby obtain a sample of greater gravity than Schrader Bluff oil. The Schrader Bluff formation underlies the Milne Point Unit located on Alaska’s North Slope. In the absence of compositional data for Ugnu, this appeared to be the best approach.

The initial compositional description of the Schrader Bluff crude oil contained 12 components, CO₂, C1, C2, C3, nC4, nC5, C6, C7-9, C10-13, C14-19, C20-35, and C36+. Properties of these components, including critical pressure, critical temperature, specific volume, and acentric factor are listed in Table 1 of reference (Guler et al, 2001). The properties of all of these components were imported into WinProp (CMG, 2004) and then lumped into several new pseudo components. Adjacent components were combined to obtain roughly equal mass fractions of the pseudo components. The initial 12 components were lumped into 4 new components: 'C1', 'C2 to C14', 'C20 to 35', 'C36+'. The names of the lumped components reflect the lumping strategy. The molecular fraction of the four components in the oil phase is 0.273, 0.423, 0.164, and 0.140 respectively. Adding two other components, H₂O and C3, we created a new six-component fluid model for simulation. PVT calculations with the lumped components, such as computation of the PT envelope, showed that the lumped component model produced virtually identical results. WinProp provides the fluid data, including the viscosity table, that are used in the input files for STARS directly. Figure 23 shows the viscosity versus temperature

correlation of the reservoir fluid. Note the more than three order of magnitude reduction in viscosity between reservoir temperature and 300 °C. The bubble point pressure is about 1170 psi and the initial solution gas-oil ratio is about 106 SCF/bbl. The oil gravity is 14.6 °API.

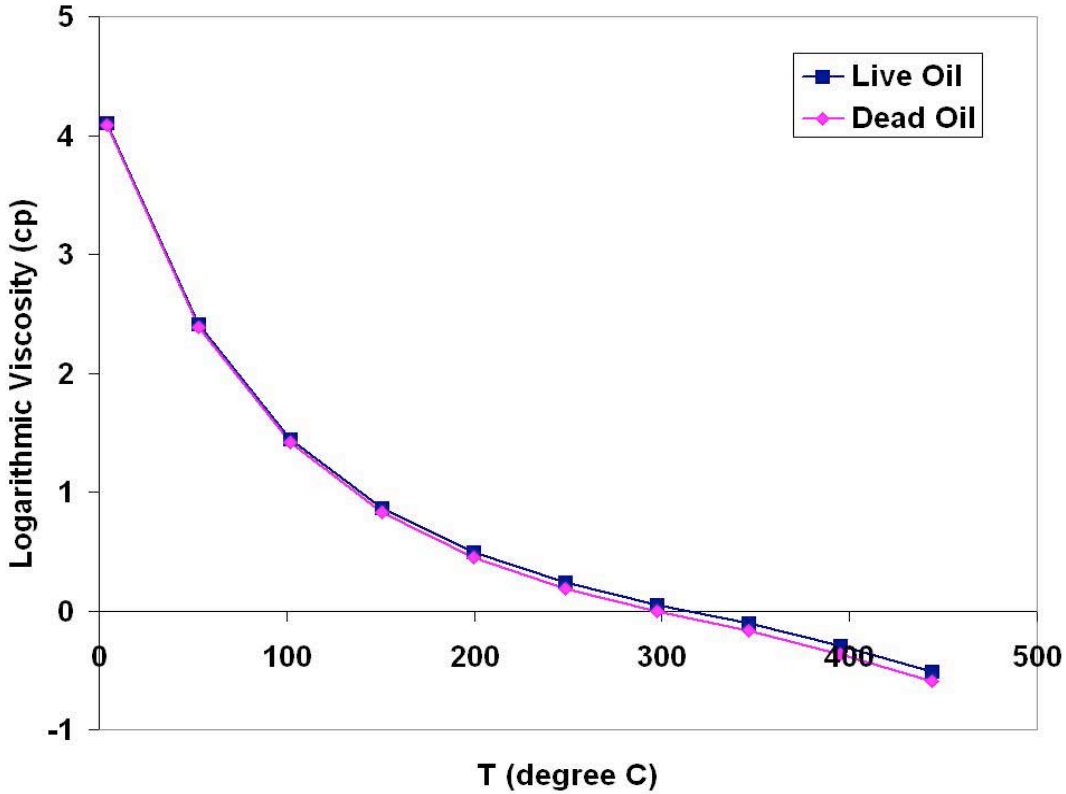


Figure 23. Logarithm of viscosity versus temperature for calculations.

Relative Permeability model: No relative permeability study has been reported for Ugnu reservoir rock. Two sets of relative permeability were used. The first is from the literature (Figures 24 and 25) and the second is hypothetical Corey-type functions (Figures 26 and 27).

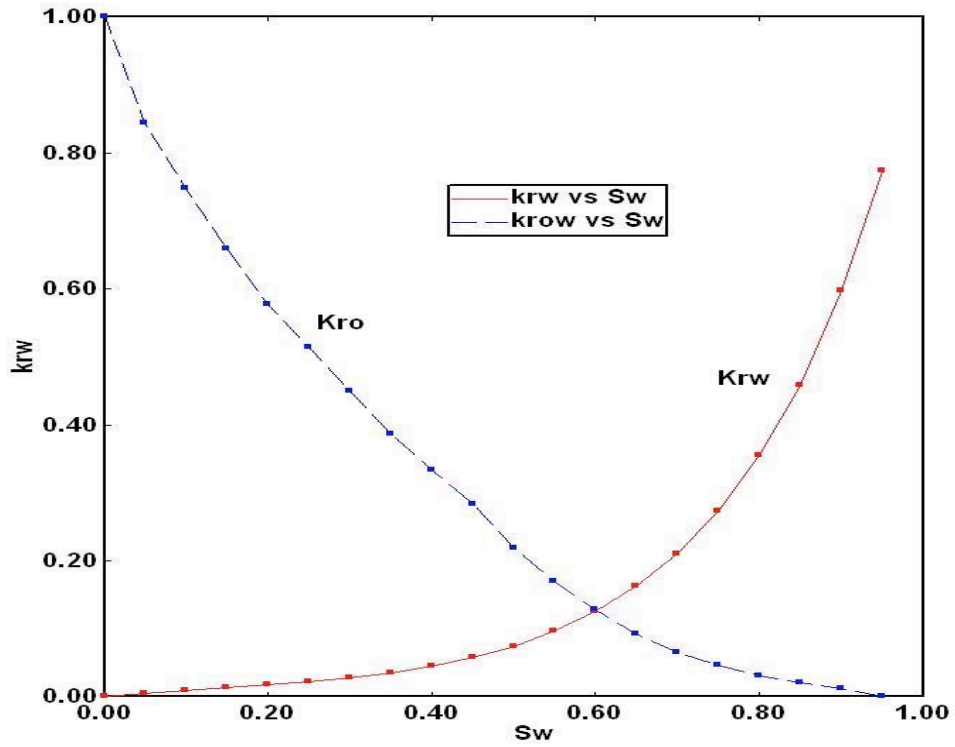


Figure 24. Water-oil relative permeability data (Hallam et al., 1991).

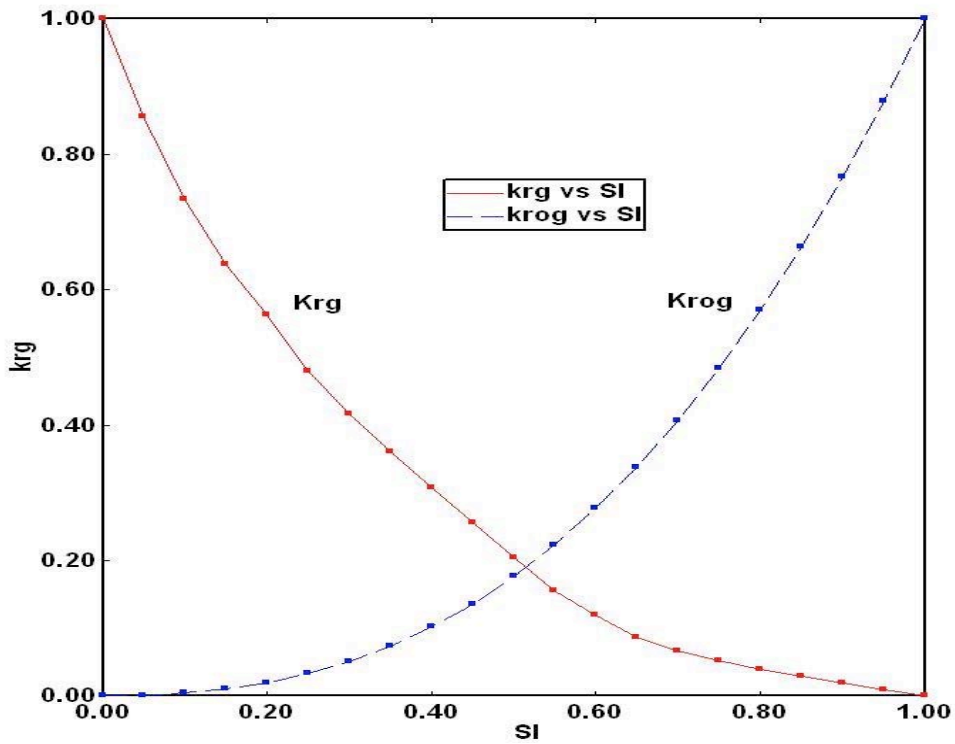


Figure 25. Gas-liquid relative permeability data (Hallam et al., 1991).

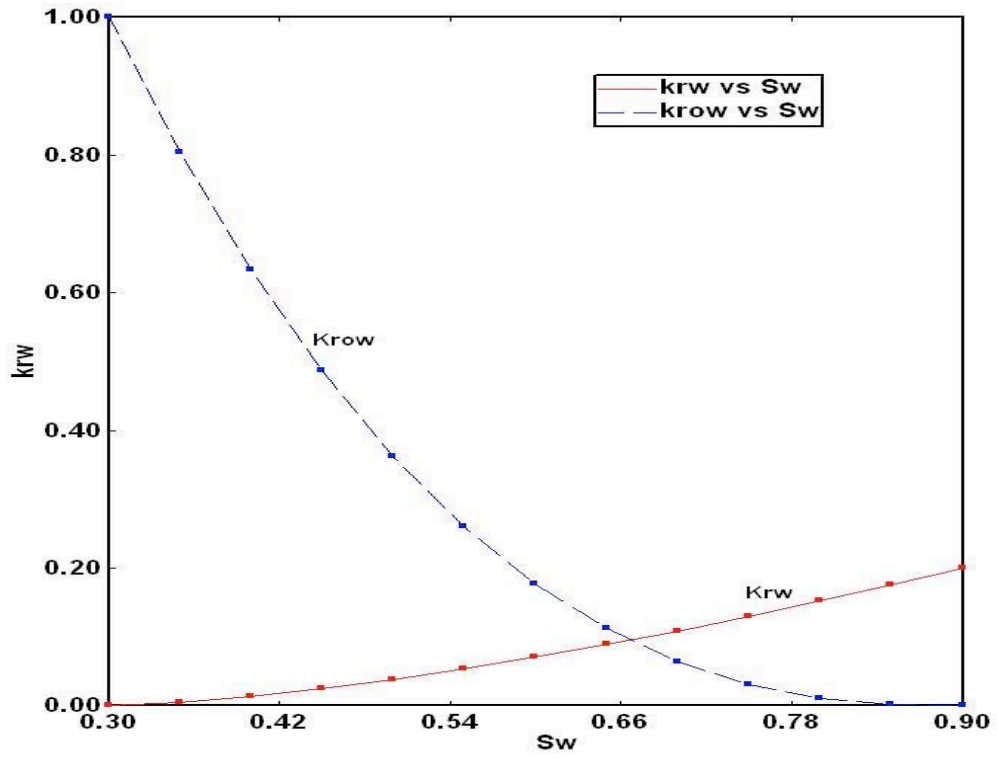


Figure 26. Water-oil relative permeability, second set, hypothetical.

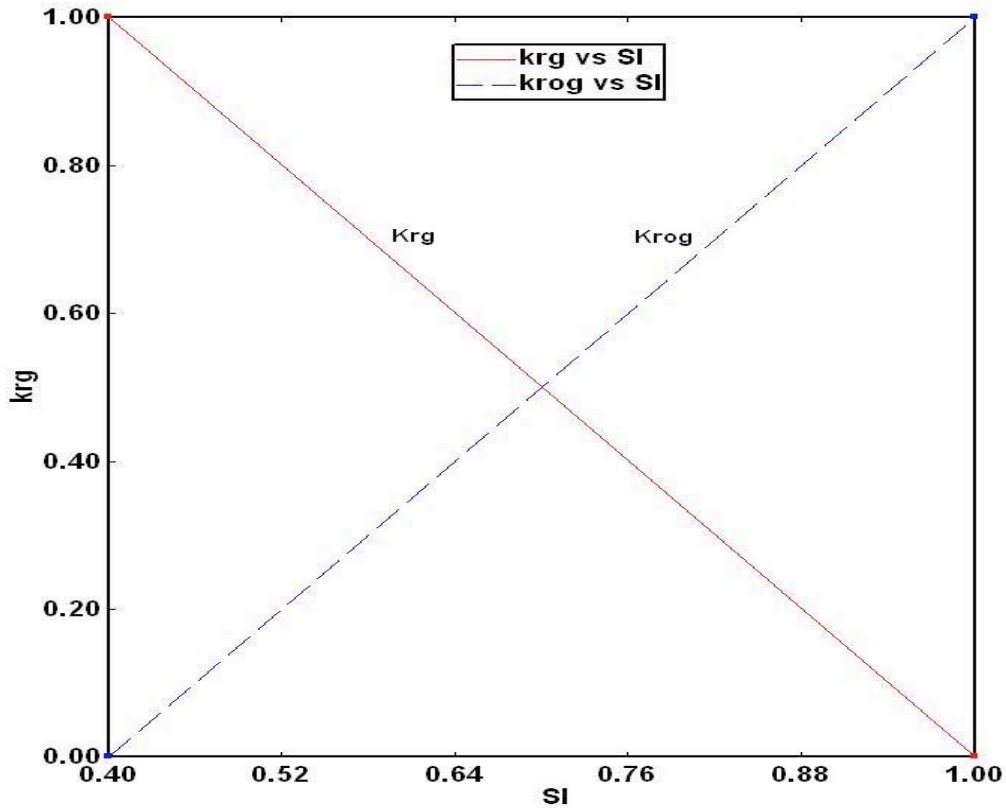


Figure 27. Gas-liquid relative permeability, second set, hypothetical.

Efficiency of different heavy-oil recovery methods

To compare the efficiency of different oil recovery methods, we designed six cases corresponding to different recovery methods as follows:

- Case 1: Single horizontal well, 4000 days of primary production.
- Case 2: Single horizontal well, 500 days of primary production and then 3500 days of electrical-heating-assisted production at a continuous heating rate of 300 BTU/ (hr/ft).
- Case 3: Single horizontal well, 500 days of primary production and then cyclic steam injection (50 days of steam injection, 10 days of shut-in, and 100 days of production for each cycle) for 22 cycles until 4000 days of production.
- Case 4: Two horizontal wells in a dual-well gravity drainage configuration, 500 days of primary production and then continuous propane injection with no heating of the injection gas for 3500 days.
- Case 5: Two horizontal wells, 500 days of primary production and then continuous propane injection that is heated electrically at 150 BTU/hr/ft for 3500 days.

- Case 6: Two horizontal wells in a dual-well SAGD configuration, 500 days of primary production and then continuous steam injection for 3500 days.

All of the above cases were run for a duration of 4000 days with the first 500 days specified as primary production. The intent of a primary-production period was to reduce reservoir pressure somewhat and establish flow into the producer. For the injection cases (SAGD, cyclic steam injection, VAPEX and heated VAPEX), a horizontal production well was located 7.5 ft above the lower boundary of the grid, and a horizontal injection well was located 20 ft above the producer. The BHPs of the injectors were all 1305 psi which was a little bit greater than the initial reservoir pressure (1300 psi); and the BHPs of the producers were 1285 psi which was slightly below the reservoir initial pressure. This producer BHP was chosen because it was believed that the main driving force for SAGD and VAPEX is gravity, therefore, we did not establish too great of a pressure difference between the injector and the producer. This pressure also kept the reservoir above its bubble point pressure. Lower producer BHPs were also tried. When the producer BHP was low, the injector BHP still needs to be somewhat high to inject steam into the reservoir. For example, when the producer BHP is 100 psi, the injector BHP should be as great as about roughly 800 psi to inject any steam at the end of the 500 days of primary production. This is because the oil is very viscous; therefore, 500 days of primary recovery did not deplete the reservoir pressure greatly. Significant pressure differences between the producer and injector gave large pressure gradients between the two wells and is not consistent with the principles of SAGD. Therefore, wells were operated at substantial pressures with some reduction in pressure over time. Initial attempts at optimizing the operating pressure are presented in the sensitivity analysis section.

Figure 27 plots the cumulative oil recovery versus energy input for the above six cases. The energy as equivalent oil and natural gas volumes are also plotted on the x axis. The conversion factor from energy to volume of oil is 5.6×10^6 BTU/bbl and from energy to volume of natural gas is 1000 BTU/SCF (Rangel-German et al., 2004). In the case of SAGD it appears that 25 bbl of oil are produced for every 1 bbl of oil input as steam energy. For cyclic steam injection and electrical heating these ratios are about 16 and 8, respectively. Recovery for the cyclic steam and electrical heating cases per unit of energy input could be substantially greater if the producer bottom hole pressure was in the range of 100 to 400 psi. Heating to reduce oil viscosity and low producer pressures makes more effective use of the reservoir's natural drive energy. Electrical heating assisted recovery and the role of producer bottom hole pressure are discussed in by Rangel-German et al, (2004).

From comparison of Figures 11 and 19, we find that SAGD has the greatest incremental oil recovery among the six cases with the same energy input, except for the primary recovery case that has no heat input. The cumulative oil recovery resulting from SAGD, was more than 6 times that of primary recovery. All of the other EOR methods including cyclic steam injection, electrical-heating-assisted recovery, heated VAPEX, and VAPEX, gave greater oil recovery than the primary case, by factors of 5, 3, 2, and 1.5 respectively. For the cyclic steam injection case, 22 cycles were conducted in total on about 160 day cycles. The duration of steam injection was fairly intensive, but is not atypical for cyclic steam injection in field applications. Although not explored explicitly, cyclic steam injection does not appear to be approaching an economic limit. That is cumulative recovery increases substantially during each cycle. The oil recovery associated with the electrical-heating-assisted method increases as the heating rate increases, as

is expected intuitively. With the same energy input, however, SAGD had greatest recovery because the injected steam helps to maintain reservoir pressure and establishes a pressure gradient throughout the reservoir.

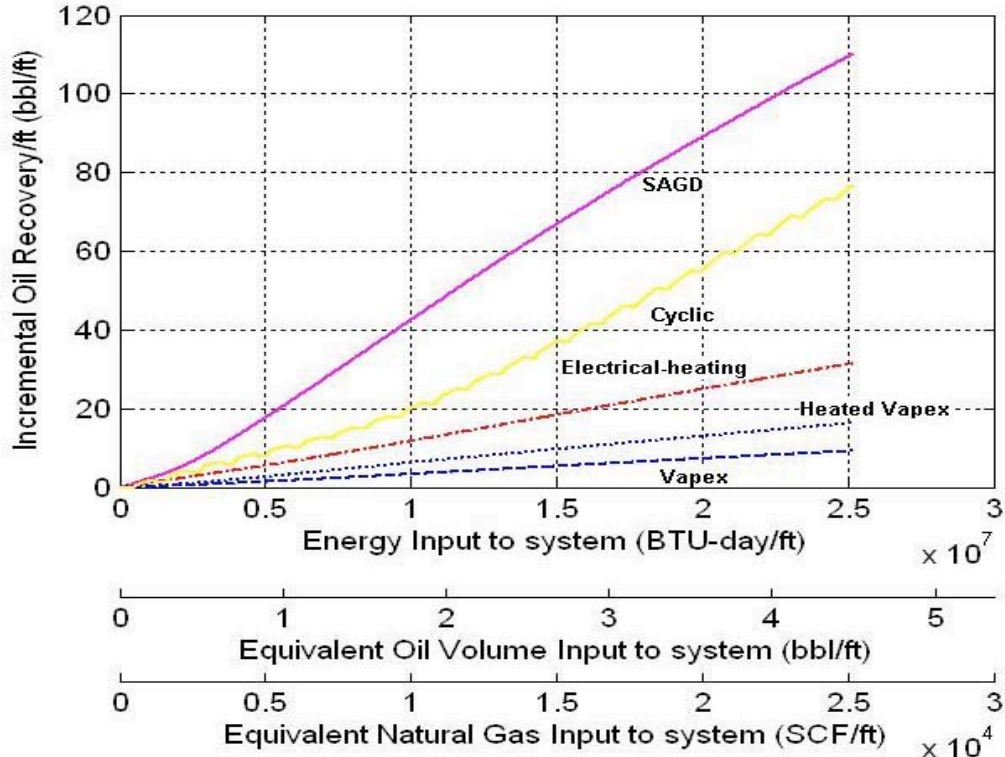


Figure 28. Incremental oil recovery versus energy input to system for all cases.

Sensitivity Study

Many factors should be considered to determine not only to choose the best method for a particular reservoir, but also what conditions to choose for a particular method to get good economics in the development of a reservoir. A sensitivity study of several parameters that were considered important in heavy-oil reservoir development was conducted in our study. The study is not exhaustive given the large number of parameters and possible cases to be run.

Location of the producer: The producer was located at different grid blocks and simulations run of the electrical-heating-assisted recovery case. For all of the cases, the BHP of the producer is 1000 psi; the heating rate is 300 BTU/hr/day. Without heat loss through the over- and under-burden formations, cumulative oil recovery decreases as the producer is raised from the bottom of the reservoir (grid block number 1, 20, 18) to the top of the reservoir (grid block number 1, 20, 2). This is because when the producer was at the bottom of the reservoir, there is more heated oil above the above the producer that was drained. When there was heat loss through the over- and under- burden formations, the well had greater cumulative oil recovery for cases with a lower position in the reservoir. The lowest position case no longer gave the greatest oil recovery due to the heat loss through the over- and under- burden formations. Given the advantage of a

bottom producer that maximizes gravity drainage forces for SAGD and VAPEX, the producer was located at the bottom of the grid (grid block number 1, 20, 18) in our simulation.

Well bottom-hole pressure: Even though all of the six cases presented in Fig. 27 used the same well constraints for ease of comparison between different recovery methods, these choices of well constraints are not necessarily the best for all of the cases. If we choose different production and/or injection conditions, the oil recovery is different for each case.

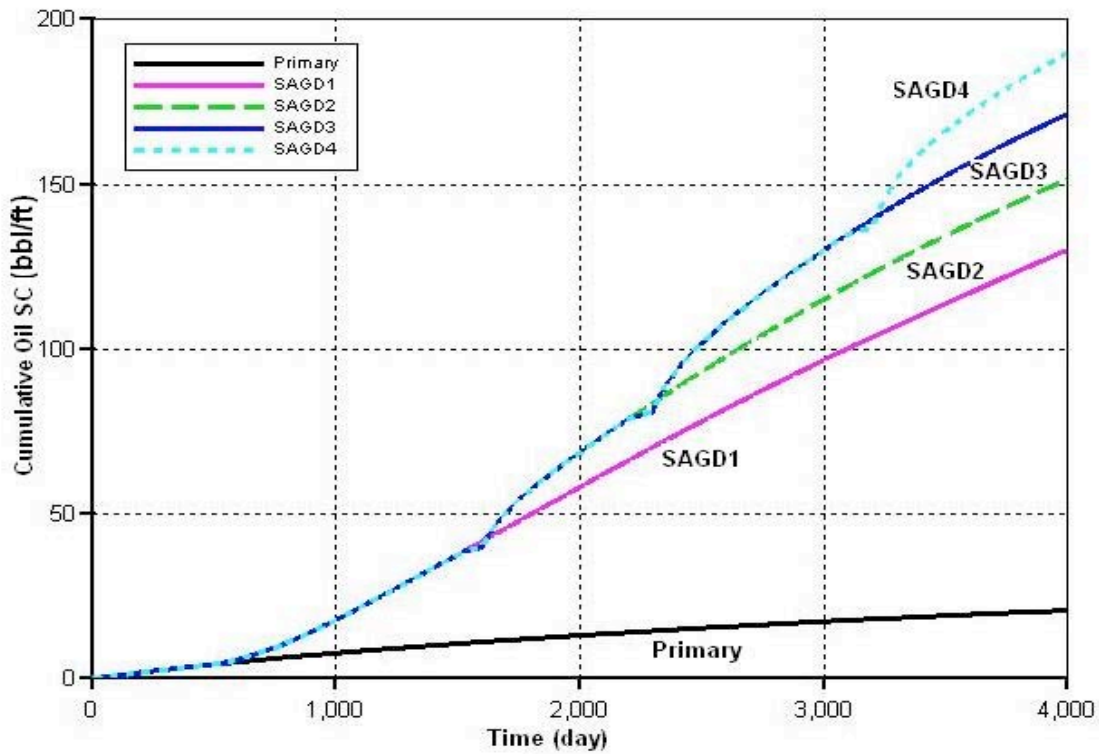


Figure 29. Cumulative recovery for SAGD cases for various producer bottom-hole pressure scenarios.

Take SAGD as an example, if we use a schedule of BHP of the producer and the injector versus time, the results are different. For the first SAGD case (SAGD 1), the BHP of producer was constant (1285 psi) during the duration of production. For the second case, (SAGD 2), the BHP of the producer was 1285 psi from the beginning to the 1600th day, and 1265 psi for the last days of production. For the third case (SAGD 3), the BHP of the producer was 1285 psi from the beginning to the 1600th day, 1265 psi from 1600th day to 2300th day, and 1245 psi for the last days of production. Similarly, for SAGD 4, the BHP of the producer was 1285 psi from the beginning to the 1600th day, 1265 psi from 1600th day to 2300th day, 1245 psi from the 2300th to the 3200th day, and 1225 psi for the last days of production. For all scenarios, the BHP difference between the producer and the injector was the same (20 psi). Figure 29 shows that the cumulative oil recovery for these different scenarios increases as the operating pressure is decreased. That is, reducing gradually the reservoir pressure over time results in greater recovery. This is not necessarily an optimized case and more aggressive reduction in pressure

over time should be possible. Optimization of pressure reduction for the other recovery methods can also be done to obtain greater recovery.

Preheating: The effect of preheating was also studied. We supposed that preheating with electrical heaters increased the oil recovery at the beginning of production and established earlier communication between the producer and the injector, and thus increased the injectivity afterwards. Figure 29 shows the cumulative oil for primary recovery and SAGD. For the primary recovery case, preheating the reservoir for the first 150 days increased the oil recovery during the period of preheating, but it did not affect recovery afterwards. A similar result was obtained for the SAGD cases. Different preheating time, either from the 1st day to the 150th day, or from the 150th day to the 300th day, or from the 350th day to the 500th day, did not give substantially different results.

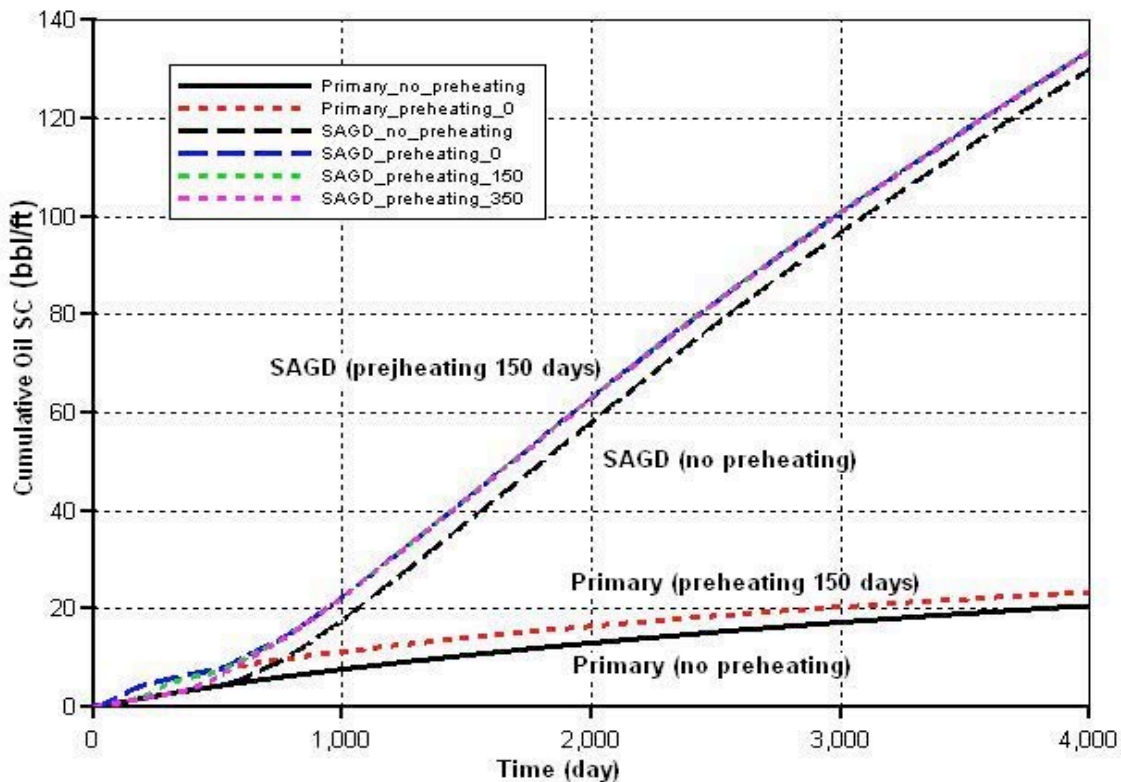


Figure 30. Effect of using electrical preheaters on SAGD performance.

Fi

For all of the SAGD cases here, the producer BHP was 1285 psi, and the injector BHP was 1305 psi which was slightly greater than the reservoir pressure. This pressure for the injector is very high. If we want to use lower injector and producer BHP without increasing the pressure drop between injector and producer, preheating is needed to establish earlier communication between the two wells and greater initial oil production. When the producer BHP was 1000 psi and the injector BHP was 1020 psi, without preheating, at the end of the first 500 days of primary recovery, the pressure near the injector was about 1160 psi. No steam could be injected at 1020 psi. With a 500-day preheating period using, however, and electrical heater in the producer and

the injector with heating rate of 600 BTU/hr/day, steam is injected. In field production when a desired injection pressure has been decided, preheating strategy, (heating rate, heating duration, etc.) can be decided accordingly.

Heterogeneity: Simulations for heterogeneous absolute permeability and porosity as mentioned above in the reservoir model part (Figure 3) were run for all of the six cases. Results (Figures 19 and 20) show that the heterogeneous cases have somewhat smaller cumulative oil recovery and oil rate for most cases.

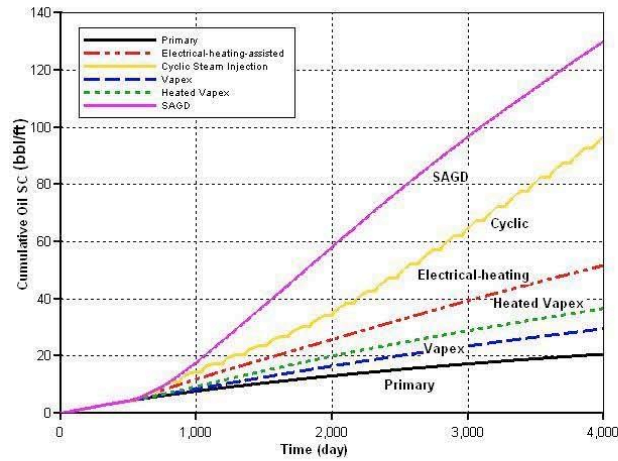
Relative permeability: Two sets of relative permeability were used in our simulation. Also, different methods to estimate three-phase relative permeability from two-phase data (STONE1, STONE 2 and Baker) were used. All cases ran equally well with each 3-phase rel-perm method. Results for different three-phase relative permeability estimation methods gave similar recovery; while results for different relative permeability sets were obviously different.

Discussion

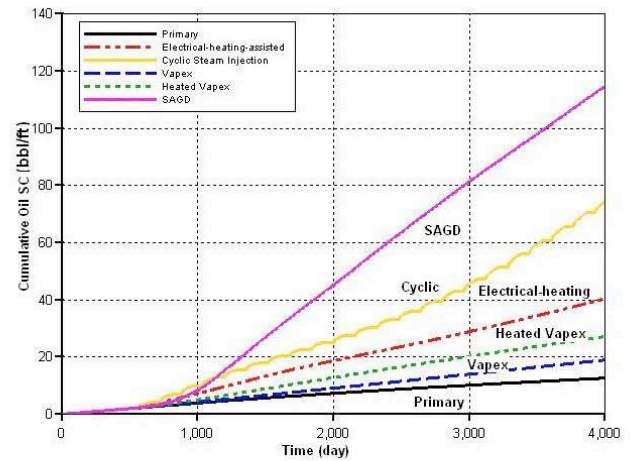
From the results of our simulation, it appears that SAGD was the most effective method to recover viscous Ugnu oil. This is largely a result of the heat delivered and the pressure maintenance associated with steam injection. In our opinion, SAGD combines the advantage of electrical-heating-assisted recovery and VAPEX. In electrical-heating-assisted recovery, the heater heated the oil around the well, which reduced the viscosity of the oil; the heated oil drained downwards to the well bore. The direction of fluid flow and the direction of heat transfer is counter current, however, and this impedes the heat transfer somewhat. In the SAGD process, the heated oil flowed downwards along the perimeter of the steam chamber and the heat was carried upward by the injected steam thereby maintaining contact with the unheated oil at the steam front. Therefore, the heat utilization was better in the SAGD process than in electrical-heating-assisted recovery. In the process of VAPEX, even though the diluted oil was also drained along the perimeter of a solvent chamber, it seemed that dilution was not as efficient as heating to reduce the viscosity of the heavy oil when the same amount of energy in the form of gas was injected.

Even though electrical-heating-assisted recovery is not as effective as SAGD in terms of the consumed energy, it deserves more attention for field application because of its relative simplicity. If a heater is placed in a production wellbore, no injection wells need to be drilled. It also seems feasible that heaters can be placed in the reservoir in a dual well configuration relatively easily. Certainly, super-insulated injection wells do not need to be installed. Likewise almost no additional surface facilities are needed for electrical-heating-assisted recovery method. Also, recovery can be further enhanced if the heater configuration and heating rate are optimized.

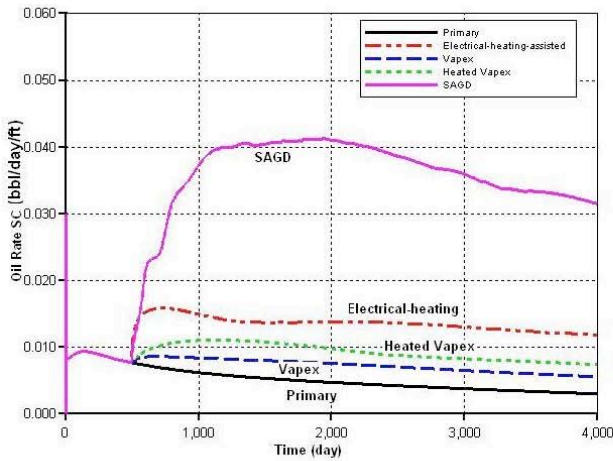
The sensitivity study concluded that well locations, well bottom-hole pressures, heterogeneity and relative permeability of reservoir rock all affected oil recovery. Therefore, these parameters should be considered not only in choosing a recovery method, but also in deciding well conditions after a recovery method has been determined. Preheating to facilitate earlier communication between the injector and producer for SAGD process was investigated. Its effect, however, did not appear to be appreciable because the oil flowed under cold conditions.



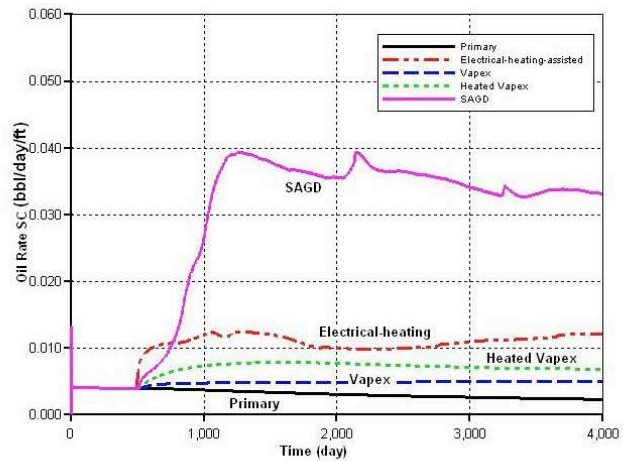
Cumulative oil recovery for homogeneous reservoir



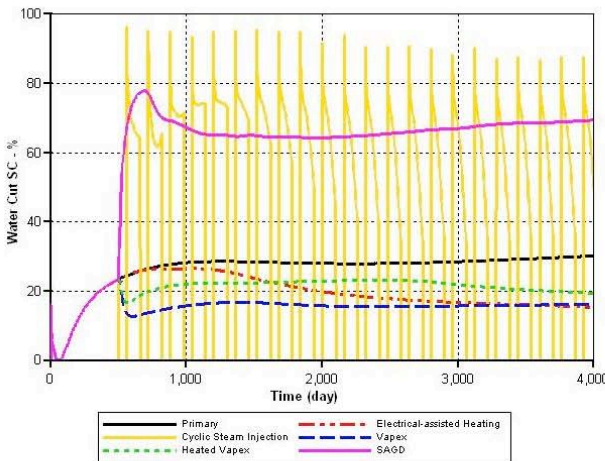
Cumulative oil recovery for heterogeneous reservoir (without correlation in any direction)



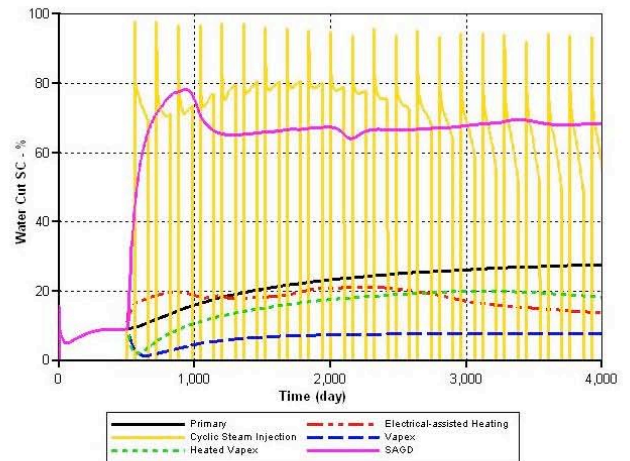
Oil production rate for homogeneous reservoir



Oil production rate for heterogeneous reservoir (without correlation in any direction)



Water cut for homogeneous reservoir



Water cut for heterogeneous reservoir (without correlation in any direction)

Figure 31. Summary of the role of heterogeneity on oil recovery performance.

2.4 Thermal Recovery–Foamed-gas mobility control

Work in the area of mobility control of steam using surfactants to create stabilized dispersed steam fell into two areas. In the first area, critical foam generation events were characterized at the pore level. These observations provided the underpinnings necessary to considering modeling of foam at the core and perhaps reservoir scale. Hence, the second area is the mechanistic modeling of foam applicable to conventional reservoir simulation. A local equilibrium approach is followed and the ability of the mechanistic approach to represent foams at high and low quality (i.e., gas fractional flow) is explored.

Foam Generation Mechanics

A series of micromodel experiments monitored via optical microscope were run to validate, or invalidate, Roof-type snap off of gas at pore throats as a foam generation mechanism. Such knowledge is important for formulation of mechanistic models of foam generation and transport in porous media. Because snap off does not require the presence of surfactant, we first omitted foamer solutions to simplify the analysis and presentation of images. Subsequent experiments have used foamer solutions to verify previous surfactant-free results.

Experiments were conducted under conditions of constant injection rates of aqueous foamer solution and nitrogen as well as constant outlet pressure. A syringe pump meters water flow at rates ranging from 0.00100 to 0.0300 cm³/min. A second syringe pump displaces water into a cylindrical transfer vessel with a gas-tight piston. Gas is thereby displaced from the transfer vessel at constant volumetric rate that varies from 0.100 to 2.000 cm³/min for gas. The micromodel is allowed to achieve steady state as gauged by a constant pressure drop as well as equality of liquid and gas injection and effluent rates. Once measurements and observations at a particular combination of flow rates are complete, new flow rates are selected and the process repeated.

A manuscript was completed, submitted for publication, and has appeared in print. Two key results are summarized by way of photographic sequences. The photographic sequences to follow focus on the same volume of pore space under identical injection conditions at gas fractional flows, f_g , equal to 0.990, as calculated at the average pressure of the micromodel. The gas injection rate is 0.4 cm³/min at standard conditions and the liquid rate is 0.00308 cm³/min. Snap off occurs over the range $0.890 < f_g < 0.993$ in a variety of pores within the micromodel that are smoothly constricted and exhibit dimensionless constriction sizes (throat:body, R_c/R_b) of roughly 0.30 or less. Above an f_g of 0.993, there is not sufficient liquid flowing at steady state for snap off to result.

The particular pore under examination is a foam germination site. Both throats connected to the pore body and present small dimensionless constriction sizes (i.e., ratio of throat to body size) that meet the static Roof criterion for snap off (Roof) and are smoothly constricted. Figure 31 documents that snap off occurs over and over again at steady state within this germination site. Again, the pore throats of interest are circled. In Fig. 31(a), the pore throat is blocked by a previously snapped off liquid lens. Figure 6(b) shows that after about 1 s the lens is displaced and coalesces leaving an pore space filled with gas. Subsequently, in Fig. 31(c) liquid rearranges to pore-spanning lenses in both of the circled throats. Figure 31(d) shows the upstream lens has coalesced after about 11 min and the downstream lens is in the process of being displaced. The downstream lens regenerates almost instantly as shown in Fig. 31(e). Once this downstream lens

coalesces a second time, snap off occurs in the upstream pore throat marked by a circle in Fig. 31(e). In summary, this germination site provides ample snapped off lenses during steady state flow that would evolve to foam lamellae if surfactant were present.

Figure 33 summarizes snap off in the micromodel in the presence of surfactant. Similar to the previous images, repeated snap off is again found. The flow direction through the pore is from right to left. A circled area in Fig. 33(a) marks the location of a pore throat blocked by a liquid lens. In Fig. 33(b), the lens is mobilized and displaced from the pore throat. Because surfactant is available to stabilize thin films, a foam lamella in the center of the pore has emerged from the displacement of the lens. Note that the pore throat in Fig. 33(b) is now open. The lamella continues to move toward the left as shown in Fig. 33(c) and is now lodged in the downstream pore throat. The upstream pore throat (circled) has undergone another snap off event and is again blocked by a liquid lens. Comparison of Figs. 33(c) and 33(d) teaches that the lamella circled in Fig. 33(c) flowed to the right upon reaching the immediate downstream branch point for flow rather than dividing into two lamellae. In Fig 33(d), the lamella has squeezed into another pore throat and is temporarily stationary.

Our micromodel observations provide compelling verification of repetitive Roof snap off in a homogeneous porous medium at steady state. Although we have focused on a single pore body connected to two throats, ample germination sites are found throughout the micromodel. For example, the pore throat connected to the wide pore body in the upper right corner of the photographs in Figs. 32 and 33 also experiences snap off. This pore exhibits a constriction to body size ratio, R_c/R_b , ratio of about 0.17 and an L/R_b ratio of 3.3 thereby meeting geometric criteria for a germination site.

We believe these new experiments to be representative of gas and water flow through sandstone reservoir media. Because repeated snap off occurs under the significantly more restrictive conditions of a 2D micromodel, then it certainly occurs in a 3D porous medium. The main restriction in 2D micromodels is sustaining two-phase flow due to the topology of the porous medium. In 2D, the average coordination number for a pore is 4, whereas it is 6 for a 3D cubic lattice. With lesser conductivity comes a reduced ability for a given pore containing gas to access wetting liquid necessary for snap off.

In general, we find the frequency of division events to be quite small in comparison to the frequency of snap off events. That is, we find scant evidence that foam generation occurs by lamella mobilization and division, as postulated elsewhere (Rossen, 2000). Note that the lamella in the upper left quadrant of Fig. 32(d) (marked with an arrow) was displaced upward from the pore throat (circled) in the lower left quadrant of the view. It does not originate from the pore discussed in Figs. 33(a) to 33(c).

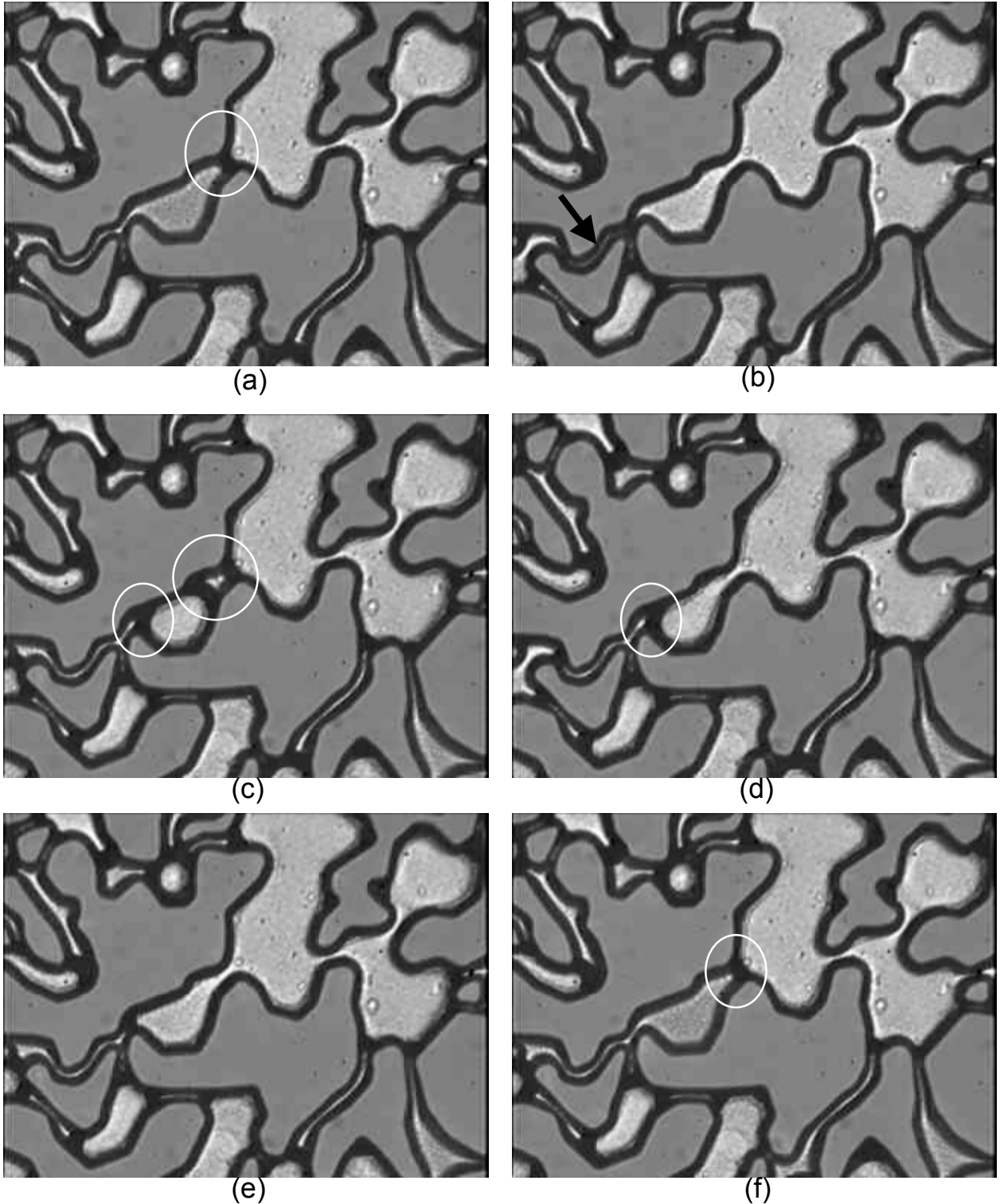


Figure 32. Repeated snap off at a germination site: (a) 0 min, liquid lens blocks pore throat, (b) 0 min-1s, lens coalesces leaving pore open, (c) 0 min-3s, snap off of gas bubble, (d) 11 min-0s, upstream lens is displaced, (e) 11 min-10 s snap off at downstream pore throat, and (f) 12 min-10 s, snap off of lens at upstream pore throat. Magnification is 200X, gas fractional flow is 0.99, and pressure drop is 227 kPa.

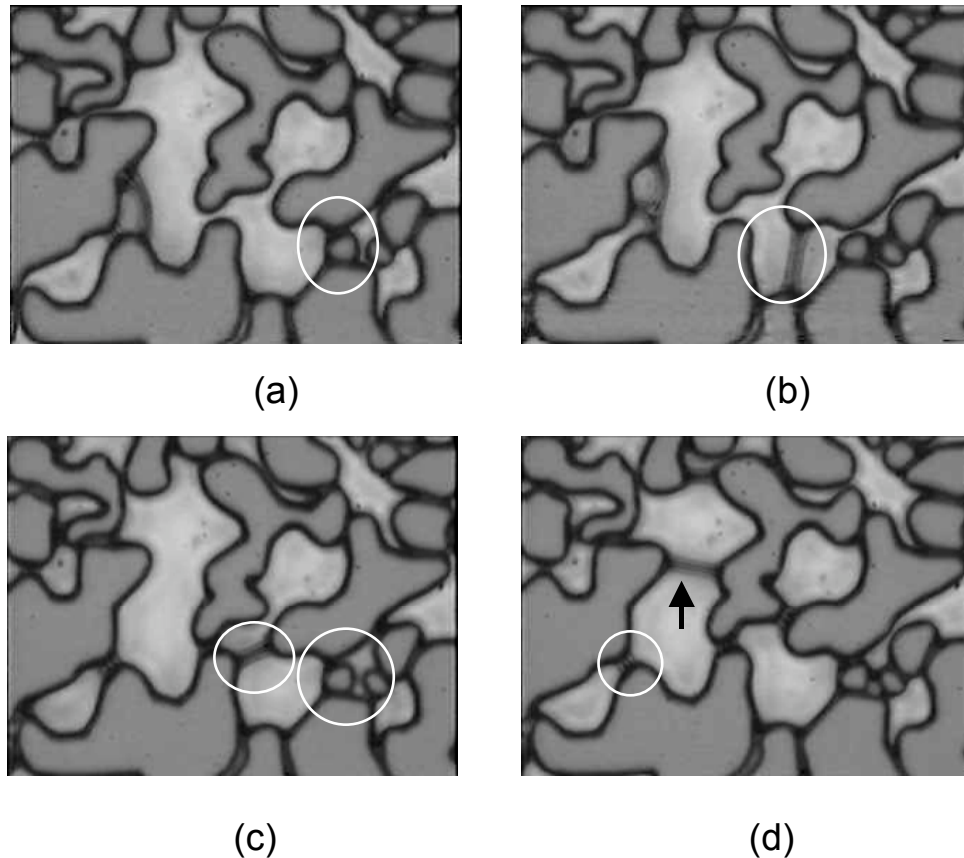


Figure 33. Snap off at a germination site: (a) 0 s, liquid lens blocks pore throat, (b) 16.2 s, lens is displaced from pore throat and evolves to a pore-spanning foam lamella, (c) 19.0 s, lamella exits pore body and reaches downstream pore throat, liqui

In summary, we find significant evidence that repeated snap off is relevant to steady-state flow through homogeneous porous media. This statement is borne out under conditions of a relatively dry porous medium at significant capillary pressure. Pore-level (Kovscek and Radke, 1996) and continuum-level population-balance models (Kovscek and Radke, 1994; Kovscek et al, 1995; Fergui et al., 1998) for foam in porous media describing and incorporating snap off mechanisms, respectively, are well founded.

Mechanistic Modeling

The second area of foamed-gas mobility control explored is continuum-level simulation. Of the various methods for gauging the effect of foam on gas mobility, we choose the population balance method for its generality and because foam texture (i.e., bubble concentration) is assessed directly. The resulting foam texture is used to obtain foamed-gas mobility reduction. In short, the population balance approach provides a framework for expressing all the relevant physics of foam generation, coalescence and transport.

A summary of the modeling framework follows as considerable details are available in the literature regarding implementation (Kovscek and Radke, 1994; Kovscek et al, 1995; Fergui et al., 1998). More detail is given where new theoretical aspects were added during this project as well as the development of the local equilibrium approach.

A material balance is written for chemical species i during multiphase flow in porous media as

$$\frac{\partial}{\partial t} \left[\phi \sum_j (S_j C_{i,j} + \Gamma_{i,j}) \right] + \sum_j \nabla \cdot \bar{F}_{i,j} = \sum_j q_{i,j} \quad (1)$$

where ϕ is porosity, S is the saturation of phase j , C is the molar concentration of species i in phase j , Γ is the adsorption of species i from phase j in units of moles per void volume, \bar{F} is the flux of species i in phase j , and q is the rate of generation of species i in phase j per unit volume of porous medium. To obtain the total mass of species i , all phases j are summed.

The net rate of foam generation is written per unit volume of gas as

$$q_f = \phi S_g \left[k_1 |\bar{v}_w| |\bar{v}_f|^{1/3} - k_{-1} |\bar{v}_f| n_f \right] \quad (2)$$

Interstitial velocities ($v_i = u_i/\phi S_i$) are local vector quantities that depend on pressure gradient and the local phase saturation. The liquid velocity dependence arises from the net imposed liquid flow through pores occupied by both gas and liquid, whereas the gas velocity dependence arises from the time for a newly formed lens to exit a pore.

The generation rate constant, k_1 , reflects the number of foam germination sites. Foam generation by snap off is mechanical in origin and for snap off to occur at a site, the site must be free of pre-existing gas bubbles. Such bubbles block the site from further foam generation. Hence, as stable, finely textured foam is generated, the likelihood of foam generation decreases. In most laboratory experiments to date strong coalescence forces, as described next, modify foam texture before foam generation is impacted. Nevertheless, reduction in foam generation as foam texture builds is reflected in the rate constant that reduces the number of germination sites as the concentration of foam bubbles increases

$$k_1 = k_1^0 \left(1 - \tanh^2 \left(\frac{n_f}{n^*} \right) \right) \quad (3)$$

where n^* is an upper limit for the concentration of foam bubbles that is related to pore size. More than one foam bubble per pore is not expected and the one bubble per pore limit sets n^* in simulations to follow. The reduction in foam germination sites as n_f becomes large allows wet foams, where the gas fractional flow is relatively low, to be simulated. Equation (3) is a new attempt to model more accurately foam generation physics. Previous modeling efforts assumed that foams were relatively dry and strong foam coalescence forces set in before bubbles became so finely textured as to reduce foam generation.

Surfactant in the aqueous phase prevents the immediate coalescence of newly formed gas bubbles by stabilizing the gas/liquid interface. At significant capillary pressure, however, surfactant fails to stabilize the interface and foam lamellae collapse. A flowing foam lamella is vulnerable to coalescence as it flows into pore space (i.e., pore bodies) where it is stretched rapidly and wetting liquid cannot flow rapidly into the lamella to prevent rupture.

Accordingly, Eq. (4) predicts that the rate of foam coalescence is proportional to the flux, $v_f n_f$, of foam lamellae into termination sites. The coalescence rate constant, k_{-1} , varies significantly with the local capillary pressure and surfactant formulation as

$$k_{-1} = k_{-1}^o \left(\frac{P_c}{P_c^* - P_c} \right)^2 \quad (4)$$

where the scaling factor k_{-1}^o is taken as a constant and P_c^* is the limiting capillary pressure for foam coalescence. Highly concentrated foamer solutions and robust surfactants lead to large P_c^* .

Experimental investigations of various aqueous surfactants suggests the following functional form for P_c^* versus surfactant concentration.

$$P_c^* = P_{c,max}^* \tanh \left(\frac{C_s}{C_s^o} \right) \quad (5)$$

where $P_{c,max}^*$ is a limiting value for P_c^* and C_s^o is a reference surfactant concentration for strong net foam generation.

In addition to bubble kinetic expressions, constitutive equations are needed for convection of foam and liquid phases. Darcy's law is retained, including standard multiphase relative permeability functions. For flowing foam, we replace the gas viscosity with an effective viscosity. Because flowing gas bubbles lay down thin lubricating films of aqueous fluid on pore walls, they do not exhibit Newtonian viscosity. The effective viscosity increases as texture increases, but is shear thinning at a constant foam textures as

$$\mu_f = \mu_g + \frac{\alpha n_f}{|\bar{v}_f|^{1/3}} \quad (6)$$

where α is a constant of proportionality that varies with surfactant formulation and permeability. As the foam texture becomes very coarse, we recover the gas viscosity.

Relative permeability of each phase is computed in the manner suggested by Kovscek et al. (1995). Foamed gas mobility is treated with an analogy to the Stone model of relative permeability. The relative permeability of the most wetting aqueous phase is a function of the aqueous phase saturation whereas the relative permeability of the foamed gas is function of only the flowing gas saturation. The functionalities of standard two-phase relative permeability functions are retained. The trapped gas saturation obviously has a relative permeability of zero.

The ability of the above new formulation for foam generation to represent high and low quality foams was then tested. Foam model parameters from the literature (Kovscek et al. 1995) were used to populate the model with input and the implementation was in a fully implicit, three dimensional reservoir simulation framework (Kovscek et al. 1997).

First, the steady state trends are examined. In some of the very earliest studies (DeVries and Wit 1990) of foam flow in porous media, it was found that the pressure drop versus flow rate behavior differed between foams created at high gas fractional flow as compared to those created at a low gas fractional flow. In the former, capillary suction controls the size of gas bubbles. Pressure drop is sensibly independent of the gas flow rate but pressure drop increases linearly with liquid flow rate. In the latter regime, the topological properties of the porous medium control bubble size (i.e., one bubble per pore). Pressure drop is then found to be sensibly independent of liquid velocity, but pressure drop increases with gas velocity.

Figure 34 plots contours of the steady-state pressure gradient as a function of the gas and liquid superficial velocity. At low liquid rate, the steady state pressure gradient is not sensitive to the gas velocity resulting in almost vertical contours, especially at liquid rates less than 0.1 m/day. On the other hand, the pressure gradient is virtually independent of liquid velocity, at fixed gas velocity, when the liquid flow rate is high. These trends result from the adjustment of bubble texture as a function of gas and liquid flow rates as embodied in Eqs. (2) through (5). When the liquid rate is small and the gas rate is fixed, foam bubbles become more finely textured as the liquid rate is increased. A more finely textured foam, at virtually the same advance rate encounters more resistance to flow, Eq. (6). For foams that are significantly wet, additional liquid injection does not change the bubble size once foam generation is limited by preexisting bubbles that block pores. Hence, the pressure gradient becomes insensitive to the liquid velocity.

Notably, the population balance model results transition smoothly from high gas fractional flow to low gas fractional flow. The trends from the literature for pressure drop versus gas flow rate are correctly predicted. It is interesting to note that although the macroscopic trends are quite different for high versus low quality foam, the constitutive equations for foamed-gas effective viscosity, relative permeability, and net foam generation are identical. The seemingly different foam rheology is predicted via the detailed accounting of foam texture versus gas and liquid flow rates without parameter adjustment.

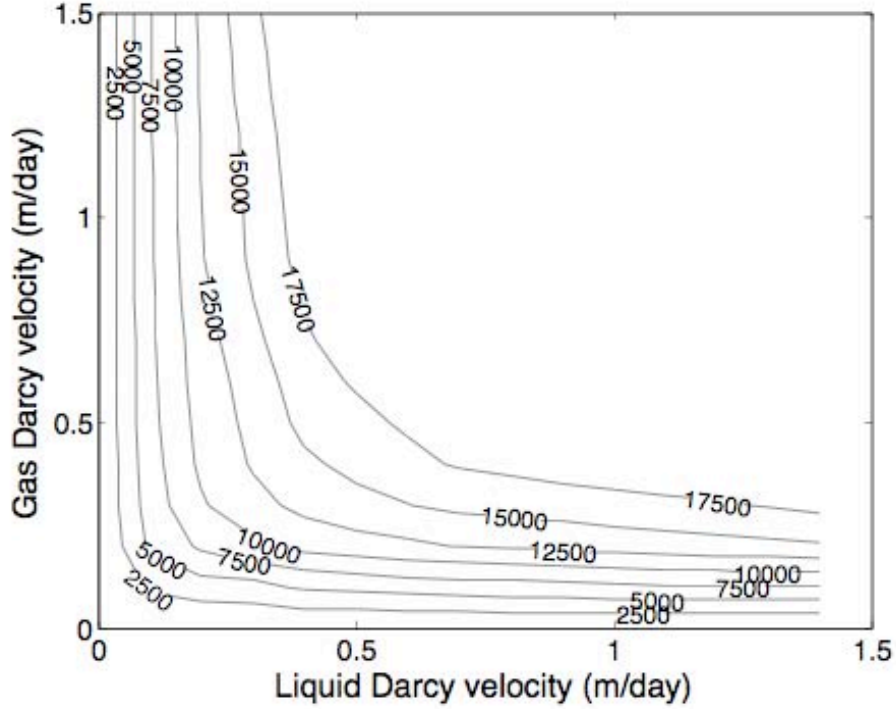


Figure 34. Contours of predicted steady state pressure gradient for foam injection into a 1.3 D sandstone. Contours are in kPa/m.

Local Equilibrium Approximation

A local equilibrium approximation to the full population balance computation of n_f may be useful for large-scale calculations as the local equilibrium solution is obtained without laborious calculations. The approximation is obtained as follows. First, the net rate of foam generation, Eq (1), is set to zero to place foam generation and coalescence rates in equilibrium:

$$\frac{n_f}{1 - \tanh^2\left(\frac{n_f}{n_*}\right)} - \frac{k_1^o |\bar{v}_w|}{k_{-1} |\bar{v}_f|^{1/3}} = 0 \quad (7)$$

Next, the hyperbolic tangent is eliminated in favor of the ratio of hyperbolic sine upon hyperbolic cosine. Subsequently, the numerator and denominator of the first term on the left of Eq (7) are multiplied by $\cosh^2(n_f/n_*)$ and the identity $\cosh^2\theta - \sinh^2\theta (=1)$ applied to yield:

$$n_f \cosh^2\left(\frac{n_f}{n_*}\right) - \frac{k_1^o |\bar{v}_w|}{k_{-1} |\bar{v}_f|^{1/3}} = 0 \quad (8)$$

The term $\cosh^2\theta (=0.25(e^\theta + e^{-\theta})^2)$ is approximated by replacing e^θ with a series approximation that is accurate to $O(\theta^4)$. That is, the series is truncated after the fourth term. After back substitution and significant simplification, the following cubic equation results.

$$n_f^3 + n_*^2 n_f - \frac{n_*^2 k_1^o |\bar{v}_w|}{k_{-1} |\bar{v}_f|^{1/3}} = 0 \quad (9)$$

The cubic equation is solved for n_f at given liquid velocity, gas velocity, and capillary pressure using standard analytical formulae (Hodgman, 1959). Stable foam requires the presence of surfactant. Hence, a simple check is made for the presence of surfactant before solving Eq. (9). If no surfactant is present, the local equilibrium foam texture is set to zero.

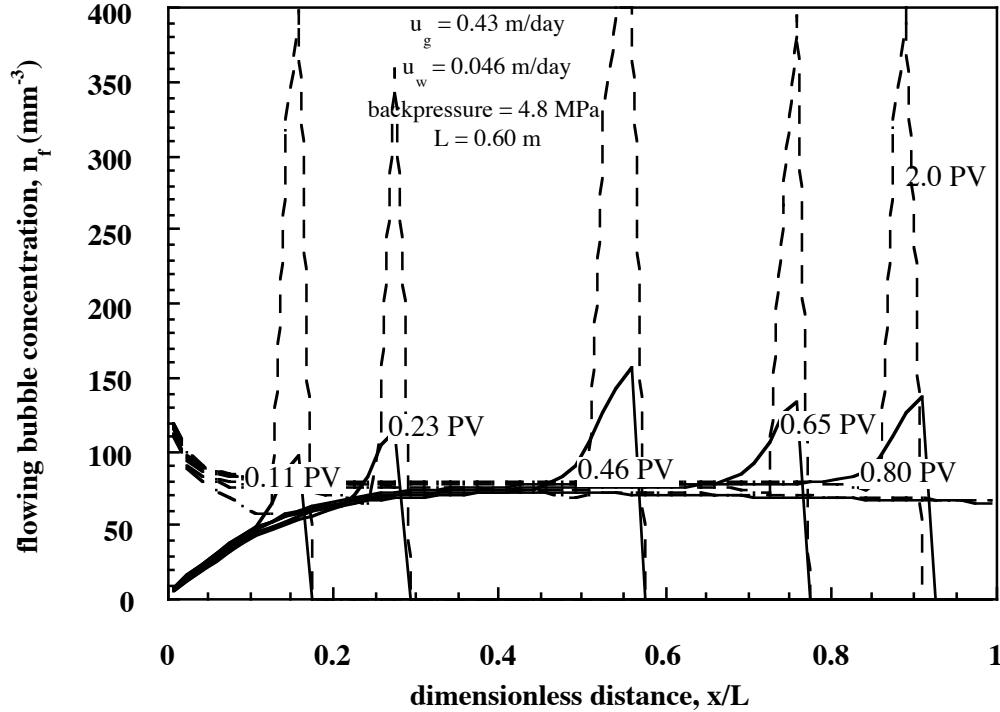


Figure 35. Local equilibrium (dashed line) and full physics population balance prediction of in-situ foam bubble concentration versus time. The core is presaturated with surfactant solution.

The applicability of the local equilibrium population balance method for foam is tested by comparing experimental results with full population balance and local equilibrium results. Two cases are given here: (1) steady liquid and gas injection into a sandstone presaturated with surfactant solution and (2) steady liquid and gas injection into a sandstone presaturated only with brine. Local equilibrium and full physics population balance results for the foam texture are computed. The experimental results are those given earlier by Kovscek et al. (1995).

Figures 35 to 37 present the computed foam texture, experimental and computed aqueous phase saturation profiles, and the computed and measured pressure drops for the case of a porous

medium fully saturated with surfactant solution. With respect to the local equilibrium and full physics representation of the foam texture in Fig. 35, good agreement between the two calculations is found except for the very small entrance region as well as immediately at the displacement front. At the front, the local equilibrium texture is significantly greater than that predicted by the full population balance method. At the relatively wet conditions at the foam displacement front, significant foam generation is favored leading to large foam textures. Downstream of the front, no gas is present and the foam textures are zero. The measured and computed aqueous phase saturation profile as well as pressure drops agree well.

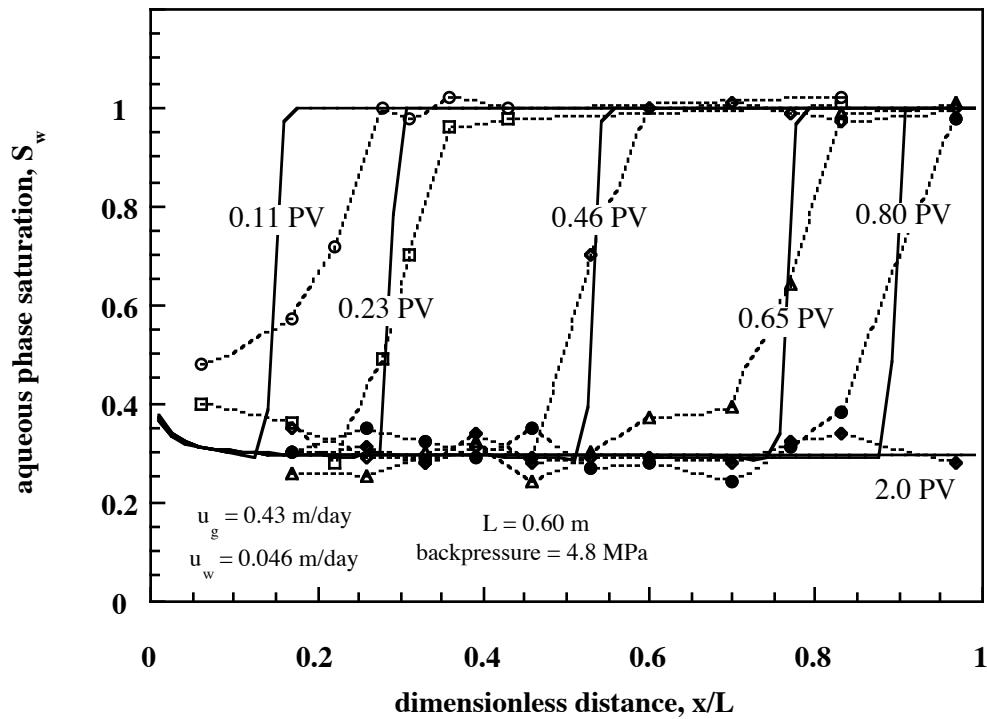


Figure 36. Measured and population balance predictions of the in-situ aqueous phase saturation history. The core is presaturated with surfactant solution.

Figures 38 to 41 present the computed foam texture, aqueous phase concentration of surfactant, experimental and computed aqueous phase saturation profiles, and the computed and measured pressure drops for the case of a porous medium fully saturated with brine but not surfactant solution. Similar to the previous case, Fig. 38 compares the local equilibrium and full physics model foam textures. A discrepancy in calculations again exists in the relatively short entrance region. This entrance region is only about 15% of the core length. Because the concentration of surfactant decreases in the flow direction, foam stability also decreases in the flow direction. Just downstream of the surfactant front, no surfactant is present in the liquid and available to stabilize

the dispersed gas phase. Hence, the foam texture declines smoothly to zero in this case. The measured and computed aqueous phase saturation profile as well as pressure drops agree well.

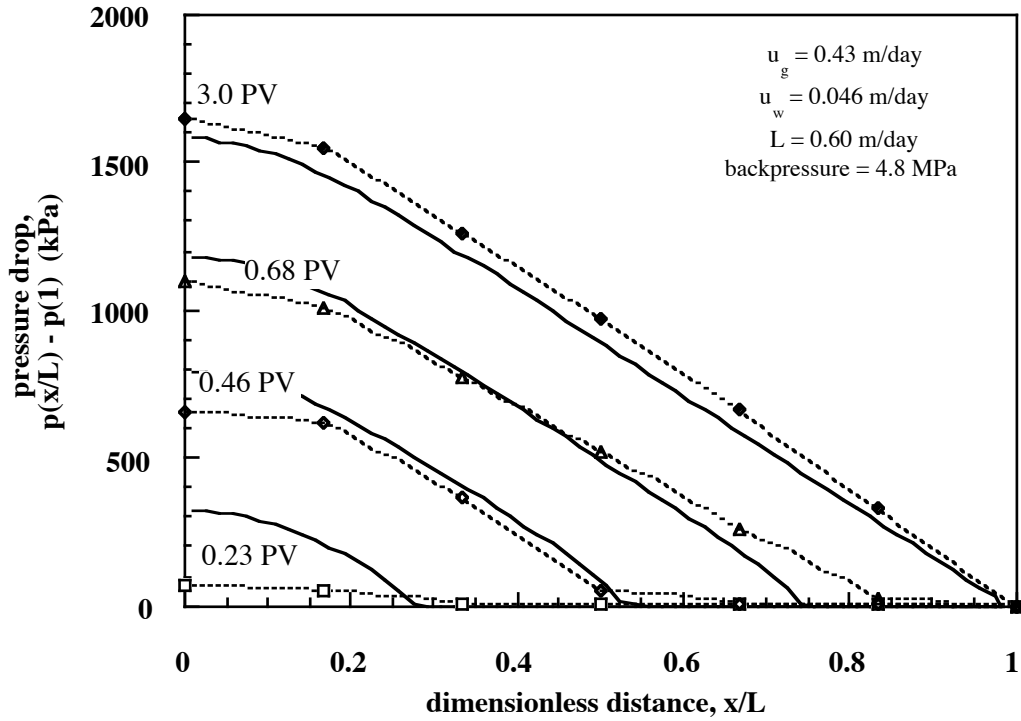


Figure 37. Measured and population balance predictions of pressure drop history for a core presaturated with surfactant solution.

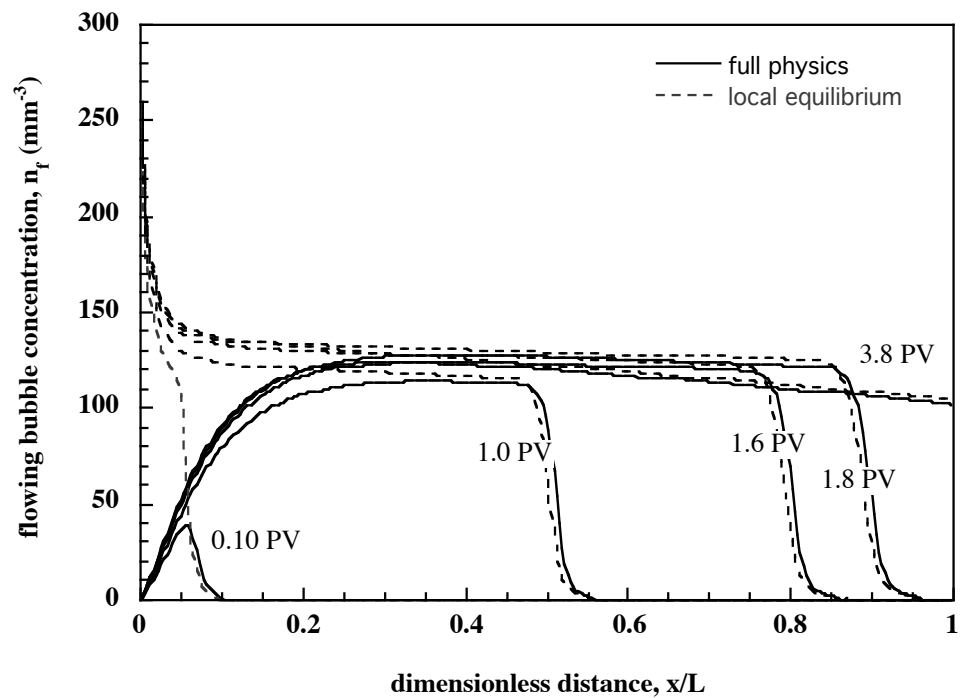


Figure 38 Local equilibrium and full physics population balance predictions of the evolution of in-situ foam texture versus time for a core presaturated with brine.

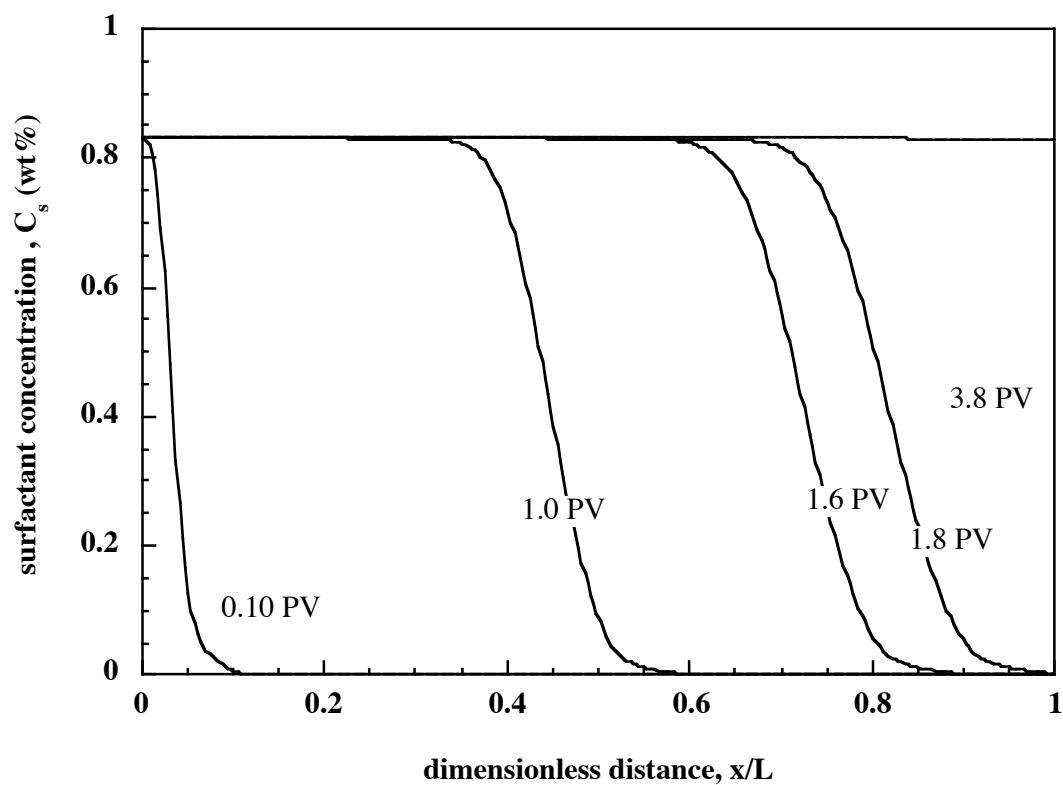


Figure 39. Computed aqueous phase concentration of surfactant.

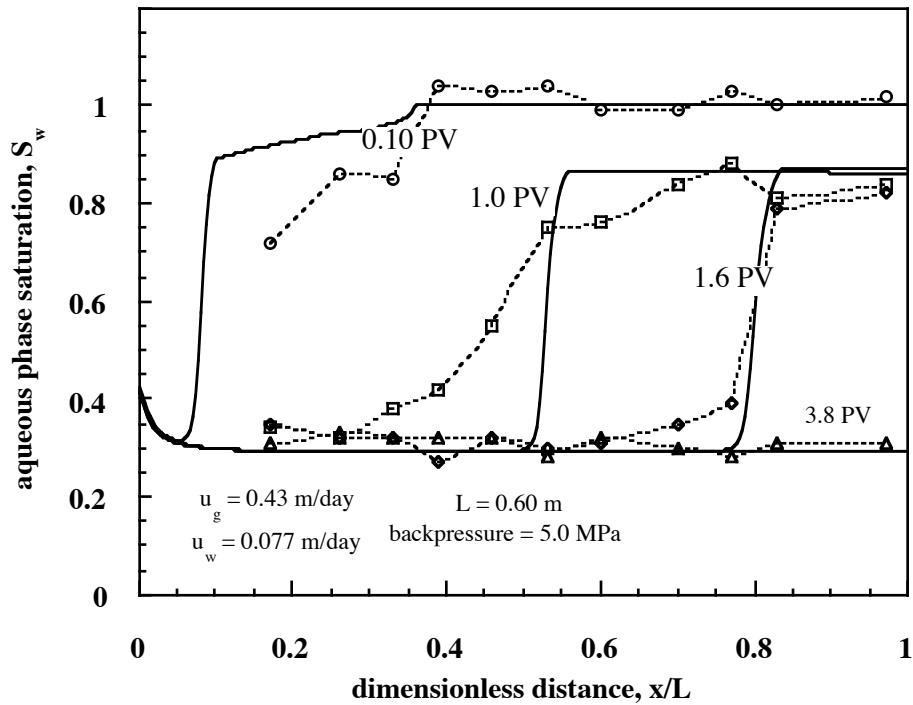


Figure 40. Measured and computed aqueous phase saturation profiles for the case of a core presaturated with brine solution.

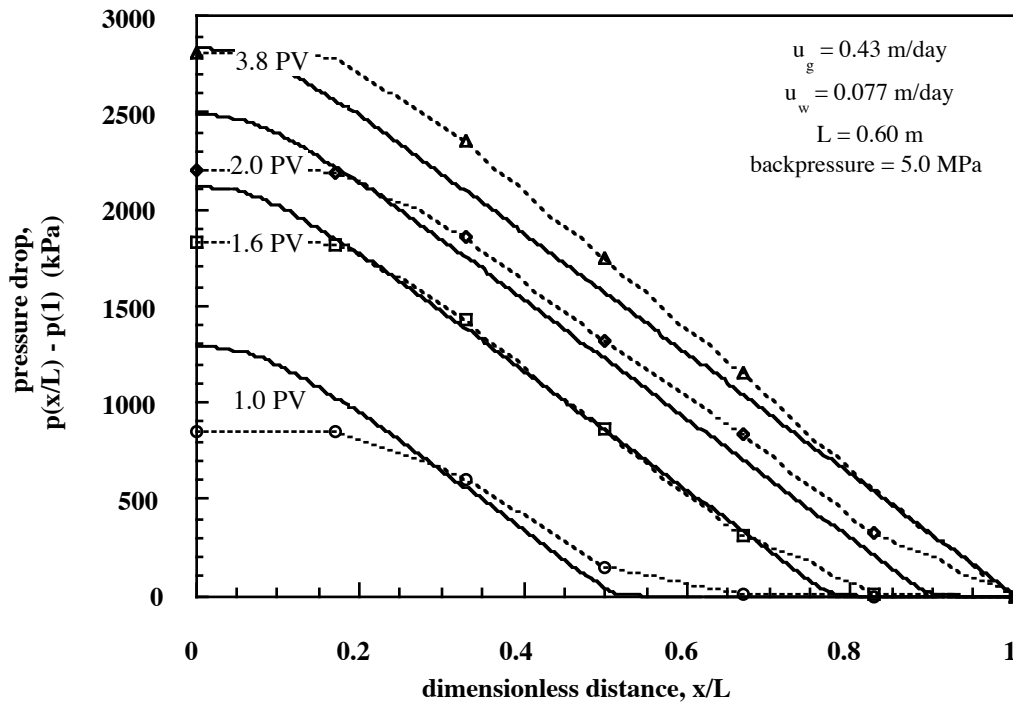


Figure 41. Measured and computed pressure drop profile histories for the case of a core presaturated with brine solution.

Management Aspects and Discussion

Cost and Schedule Status

At the end of year 2, work was on schedule and on budget. Cost details are provided separately by the Stanford Sponsored Projects Office.

Summary of Accomplishments

Given the limits on available funding, this project is only two-thirds complete in a chronological sense. Technical accomplishment, however, is not a linear process. The majority of project tasks and subtasks were parallel, with significant linkage among subtask, rather than sequential. Year 3 activities were clearly critical to meeting project goals.

Progress toward the goal of providing a suite of midterm research needed to produce effectively the abundant, discovered heavy-oil resources of the United States was clearly made. A spectrum of applicable enhanced recovery processes was identified and tested in a preliminary sense using thermal reservoir simulation. Generally, electrothermal, conventional steam-based, and thermal gravity drainage enhanced oil recovery techniques appear to be applicable to “prime” Ugnu reservoir conditions to the extent that reservoir architecture and fluid conditions are modeled faithfully here.

Specific accomplishments follow:

- Publication of a manuscript entitled, “Verification of Roof Snap Off as a Foam Generation Mechanism in Porous Media at Steady State,” by A. R. Kovscek, G.-Q. Tang, and C. J. Radke, *Colloids and Surfaces A: Physicochemical and Engineering Aspects*(Physicochemical and Engineering Aspects); 20 July 2007, 303 (1-3), .251-60.
- Presentation of a manuscript entitled, “The Role of Oil Chemistry on Cold Production of Heavy Oils,” SPE 102365 by G.-Q. Tang, C. Temizel, and A. R. Kovscek, Proceedings of the SPE Annual Technical Conference and Exhibition, San Antonio TX, Sep 24 – 27, 2006.
- Presentation of " Effects of Reservoir Heterogeneities on the Steam-Assisted Gravity Drainage Process," SPE 109873 by Chen, Q., M.G. Gerritsen, and A. R. Kovscek, Proceedings of the SPE Annual Technical Conference and Exhibition, Anaheim, CA. Nov. 11 - 14, 2007.
- Publication of the manuscript " Effects of Reservoir Heterogeneities on the Steam-Assisted Gravity Drainage Process," SPE 109873 by Chen, Q., M.G. Gerritsen, and A. R. Kovscek, *Society of Petroleum Engineers Reservoir Evaluation & Engineering*, to appear 2008.

Actual or Anticipated Problems

To date there has been only a single problem related to obtaining an oil sample from the Ugnu reservoir of significant volume for heavy-oil depletion experiments. Industry partners attempted for about two years to supply us with an uncontaminated sample. Efforts actually predate the beginning of this contract. Their pumps, however, have suffered from numerous sanding and

other operational problems. This situation was beyond our control. Rather than wait longer, the work plan was modified to examine viscous West Sak crude under representative conditions.

Several smaller samples from Ugnu were obtained and analyzed.

Technology Transfer Activities

- Heavy-oil project team members attended the Society of Petroleum Engineers Annual Technical Conference and Exhibition, Los Angeles, CA , Nov. 11 – 14, 2007
- A 4-day long short course on thermal and heavy-oil recovery was taught July 9 to 12, 2007 at Stanford University. The target audience was practicing engineers and geologists. This offering attracted 11 attendees.
- Heavy-oil project team members attended the Society of Petroleum Engineers Annual Technical Conference and Exhibition, San Antonio TX, Sep 24 – 27, 2006.
- A 4-day long short course on thermal and heavy-oil recovery was presented August 22 to 25, 2006 at Stanford University. There were 7 attendees.
- A heavy-oil and thermal recovery workshop was held May 1 and 2, 2006 on the campus of Stanford University. The purpose of the meeting was to present research results to and garner suggestions/input from industry researchers, technology developers, and technology implementers. Representatives from Aera Energy LLC, Berry Petroleum, BP Exploration (Houston), ChevronTexaco, ConocoPhillips, Japan National Oil Corporation, RIPED PetroChina, Shell International E&P (Houston), and Total. were in attendance.
- A. R. Kovscek presented a talk on January 25, 2006 at the Woods Institute for the Environment Energy Seminar entitled "Heavy-Oil Hydrocarbon Resources: Their Production and the Resulting CO₂ Footprint."
- Heavy-oil project team members attended the Society of Petroleum Engineers / Department of Energy Improved Oil Recovery Symposium, Apr 22-26, 2006 in Tulsa, OK.
- A. R. Kovscek visited the offices of BP Exploration Alaska in Anchorage on March 21, 2005 for discussion and to make a presentation entitled "Heavy-Oil and Thermal Recovery Research Activities at Stanford University."
- Heavy-oil project team members attended the Society of Petroleum Engineers Western Regional Meeting March 30 to April 1 in Irvine, CA.
- Semiannual Technical Progress Report for the Reporting Period October 1 2004 – March 31, 2005 was submitted to Document Control.
- At the invitation of BP Exploration Alaska, A. R. Kovscek attended a Viscous Oil Symposium held in Girdwood, AK from May 24 to 26, 2005. He made a presentation entitled: "Viscous Oil Recovery Mechanisms: Cold to Thermal Production"

- A 4-day long short course on thermal and heavy-oil recovery was taught June 27 to 30, 2005 at Stanford University. The target audience was practicing engineers and geologists. This year's offering attracted 13 attendees.
- A heavy-oil and thermal recovery workshop was held April 19 and 20, 2005 on the campus of Stanford University. The purpose of the meeting was to present research results to and garner suggestions/input from industry researchers, technology developers, and technology implementers. Representatives from Aera Energy LLC, Berry Petroleum, BP Exploration (Houston), ChevronTexaco, ConocoPhillips, RIPED PetroChina, Shell International E&P

Conclusion

Two of the three planned project years for, “Transformation of Resources to Reserves: Next Generation Heavy Oil Recovery Techniques” were completed. Research was well underway to provide the technical foundations needed to produce efficiently U.S. discovered, abundant, heavy-oil resources when the project was stopped. In essence, the work was only two-thirds complete and the following observations should be treated as tentative or incomplete.

If the project had proceeded to completion, the knowledge base for cold primary production and enhanced recovery by thermal methods would have been extended significantly. We were well on the way to developing an understanding of the chemical functional groups as well as oil composition that leads to so-called foamy oil behavior and significant cold production. While many surface and facilities issues clearly exist with respect to thermal recovery of heavy oil in cold environments, including effect insulation of wells, this project has established tentative feasibility from a subsurface perspective for thermal recovery of heavy oil in such cold environments. Although there are few commercially available options, sufficient means to protect the environment from hot well bores have been described technically. Thermal recovery options of cyclic steaming injection, thermal gravity drainage, and downhole electrical heaters all appear to yield significant incremental recovery of viscous oil. Process economics were not in the scope of this project. Hydraulic fracturing of horizontal injectors hold much promise for improving steam injectivity and the distribution of steam in heterogeneous sands.

Specific conclusions include:

- a knowledge base with respect to thermal well completions exists and is available for development in cold environments,
- chemical analysis of heavy and viscous oils display considerable variation in acid and base numbers and these differences appear to be indicators of oils that present favorable recovery characteristics by heavy-oil solution gas drive,
- depletion tests using recombined West Sak crude oil yielded about 20% of the OOIP independent of system parameters.
- a semianalytical model for cyclic steaming in horizontal wells was developed and validated,
- hydraulically fractured horizontal wells appear to offset adverse vertical permeability enabling steam distribution and gravity drainage of heavy oil,
- experiments that analyze foam generation mechanisms in micromodels validate prior work that asserted snap off as a dominant foam generation mechanism,

- aqueous foams may be viable for mobility control of steam and initial attempts to reduce the mechanistic population balance simulation approach for foam to a local equilibrium expression with significantly reduced computational requirements are positive and this area should be examined further.

References

- Afkhhampur, K.H, 1985. "A Novel Approach to Solving Downhole Fluid Flow Problems by Use of an Electric Heating System," IEEE Trans. 225-235 (Paper No. PCIC-85-35).
- Akin, S. and A. R. Kovscek, 2002. "Heavy Oil Solution Gas Drive: A Laboratory Study," *Journal of Petroleum Science and Engineering*, **35(1-2)**, 33-48.
- ASTM–American Society of Testing and Measurement, 2006. "Annual Book of ASTM Standards. Volume 5 Petroleum Products and Lubricants," ASTM: West Conshohocken, Pennsylvania D664-01, D2896-95.
- Aziz, K. and Gontijo J.E., 1984. "A Simple Analytical Model for Simulating Heavy Oil Recovery by Cyclic Steam in Pressure-Depleted Reservoirs", paper SPE 13037 presented at the 59th Annual Technical Conference and Exhibition, Houston (September 16-19, 1984).
- Bulter. R. M, and Mokrys, I. J., 1991. "A New Process (VAPEX) for Recovering Heavy Oils Using Hot Water and Hydrocarbon Vapor," J. Can. Pet. Tech (Jan-Feb.) 30(1), 97-106.
- Callaghan, I. C., McKetchnie, A. L., Ray, J.E., and Wainright, J.C., 1985 "Identification of Crude Oil Components Responsible for Foaming," Soc, Petr. Eng. J. , 25(2), 171-175.
- CMG—Computer Modeling Group, 2004. STARS User Manual, Calgary, Alberta Canada.
- De Vries, A.S. and Witt, K, 1990. Rheology of Gas/Water Foam in the Quality Range Relevant to Steam Foam, *Society of Petroleum Engineers Reservoir Engineering*, 5, 185-192.
- Dullien, F.A.L., 1992. *Porous Media: Fluid Transport and Pore Structure*, 2nd Ed., Academic Press, Sand Diego, CA.
- Edmunds, N. R., 1998. "Investigation of SAGD Steam Trap Control in Two and Three Dimensions", SPE 50413, SPE International Conference on Horizontal Well Technology, Calgary, Alberta, Canada.
- Egermann, P., Renard G. and Delamaide E, 2001."SAGD Performance Optimization through Numerical Simulations: Methodology and Field Case Example", SPE 69690. SPE International Thermal Operations and Heavy Oil Symposium},Porlamar, Margarita Island, Venezuela.
- EIA (2003). "Annual Energy Review" Energy Information Administration, Washington DC, www.eia.doe.gov/emeu/international/gas.html.
- Elliot, K. T. and A. R. Kovscek, 2001."A Numerical Analysis of the Single-Well Steam Assisted Gravity Drainage Process," *Petroleum Science and Technology*, **19(7&8)**, 733-760.
- Fergui, O., H. Bertin, M. Quintard, 1998. Transient aqueous foam flow in porous media: experiments and modeling, J. Petr. Sci & Eng. 20 9-29.
- George, D. S., O. Hayat, and A. R. Kovscek, 2005."A Microvisual Study of Solution Gas Drive Mechanisms in Viscous Oils," *Journal of Petroleum Science and Engineering*, **46(1-2)**, 101-119. DOI: 10.1016/j.petrol.2004.08.003.
- Guler, B., P. Wang, M. Delshad, G. A. Pope, and K. Sepehrnoori, 2001, "Three- and Four-Phase Flow Compositional Simulations of CO₂/NGL EOR," SPE 71485, presented at the 2001

- SPE Annual Technical Conference and Exhibition, New Orleans, Louisiana, 30 September–3 October 2001.
- Hodgman, C. D (ed) 1959. *CRC Standard Mathematical Tables*, 12th Edition. Cleveland OH: Chemical Rubber Publishing Co. 525 pp.
- Hornbrook, J.W., Castanier, L.M. and Petit, P.A. 1991. "Observation of Foam/Oil Interactions in a New, High-Resolution Micromodel", paper SPE 22631 in Proceedings of the SPE Annual Technical Conference and Exhibition, Dallas, TX, October.
- Hubbert, M.K. and Willis D.G., 1957. "Mechanics of Hydraulic Fracturing", *Pet Trans AIME*, 210, 153–163.
- Janisch, A (1979). "Oil Sands and Heavy Oil: Can They Ease the Energy Shortage?" 1st UNITAR International Conference on Heavy Crude and Tar Sands, Edmonton, Alberta, June 4-12.
- Kovscek, A. R. and C. J. Radke, 1994. "Fundamentals of Foam Transport in Porous Media," in *Foams: Fundamentals and Applications in the Petroleum Industry*, Schramm, L. L. Ed., ACS Advances in Chemistry Series No. 242, American Chemical Society, Washington D.C., 115-163.
- Kovscek, A. R., T. W. Patzek, and C.J. Radke, 1995. "A Mechanistic Population Balance Model for One Dimensional Foam Flow in Boise Sandstone," *Chemical Engineering Science*, 50(23), 3783-3799.
- Kovscek, A. R., T. W. Patzek, and C. J. Radke, 1997. "Mechanistic Foam Flow Simulation in Heterogeneous and Multidimensional Porous Media," *Society of Petroleum Engineers Journal*, 2(4), 511-526.
- Kovscek, A. R., and C. J. Radke, 1996. "Gas-Bubble Snap-Off Under Pressure Driven Flow in Constricted Noncircular Capillaries," *Colloids and Surfaces A: Physicochemical and Engineering Aspects*, 117, 55-76.
- Kovscek, A. R. and Castanier, L. M., 2005. "Transformation of Resources to Reserves: Next Generation Heavy-Oil Recovery Techniques", Semiannual Technical Progress Report Reporting Period October 1 2004 – March 31, 2005.
- Kovscek, A. R. and Castanier, L. M., 2005. "Transformation of Resources to Reserves: Next Generation Heavy-Oil Recovery Techniques", Semiannual Technical Progress Report Reporting Period April 1, 2005 – September 30, 2005.
- Liang, L., 2005, "An Analytical Model for Cyclic Steaming of Horizontal Wells" M.S. Report Stanford University. online: <http://geothermal.stanford.edu/pereports/search.htm>
- Mahmood, S. M., Olsen, D. K. and Thomas, C. P. (1995). Heavy Oil Production from Alaska. R. F. Meyer. 6th UNITAR International Conference on Heavy Crude and Tar Sands, Houston, TX, February 12-17.
- Marques, C. 2007. Thaw Front Dynamics of Superinsulated Wells in Cold Environments. MS Thesis, Stanford University. <http://pangea.stanford.edu/ERE/db/pereports/search.html>
- Moridis, G. (2002). "Worldwide EOR Survey", *Oil and Gas J.*, Apr. 20, 49-97.
- Myhill, N.A. and Stegemeier, G.L., 1978. "Steam Drive Correlation and Prediction", *J. Pet. Tech.* (February) 173-182.
- Rangel-German, E. R., J. Schembre, C. Sandberg, A.R. Kovscek, 2004. "Electrical-heating-assisted recovery for heavy oil," *Journal of Petroleum Science and Engineering* 45 213-231.
- Rossen, W. R., 2000. "Snap off in Constricted Tubes and Porous Media," *Colloids and Surfaces A*, 166, 101-107.

- Sagar, N.S. and Castanier, L.M. 1998. "Pore-Level Visualization of Oil/Foam Oil-Foam Interactions in a Silicon Micromodel", paper SPE 39512 in Proceedings of the SPE/DOE Improved Oil Recovery Symposium, Tulsa, OK, April.
- Speight, J. 1999. *The Chemistry and Technology of Petroleum*, 3rd Ed. New York: Marcel Dekker.
- Tang, G.-Q., Temizel, C., and Kovscek, A. R. 2006. "The Role of Oil Chemistry on Cold Production of Heavy Oils," SPE 102365, Proceedings of the SPE Annual Technical Conference and Exhibition, San Antonio TX, Sep 24 – 27, 2006.
- Vittoratos, E. S., Brice, B. W., West, C. C., Diger, S. A., and Chambers, B.C., 2006, "Optimizing Heavy Oil Waterflooding: Are the Light Oil Paradigms Applicable?", Paper 2006-688, Proceedings of the 1st World Heavy Oil Conference, Beijing China.
- Zhou, Z. A., Xu, Z., Masliyah, J. H., and Czarnecki, J., 1999. "Coagulation of Bitumen with Fine Silica in Model Systems," *Colloids and Surfaces A*, 148, 1999.

National Energy Technology Laboratory

626 Cochrans Mill Road
P.O. Box 10940
Pittsburgh, PA 15236-0940

3610 Collins Ferry Road
P.O. Box 880
Morgantown, WV 26507-0880

One West Third Street, Suite 1400
Tulsa, OK 74103-3519

1450 Queen Avenue SW
Albany, OR 97321-2198

539 Duckering Bldg./UAF Campus
P.O. Box 750172
Fairbanks, AK 99775-0172

Visit the NETL website at:
www.netl.doe.gov

Customer Service:
1-800-553-7681

